

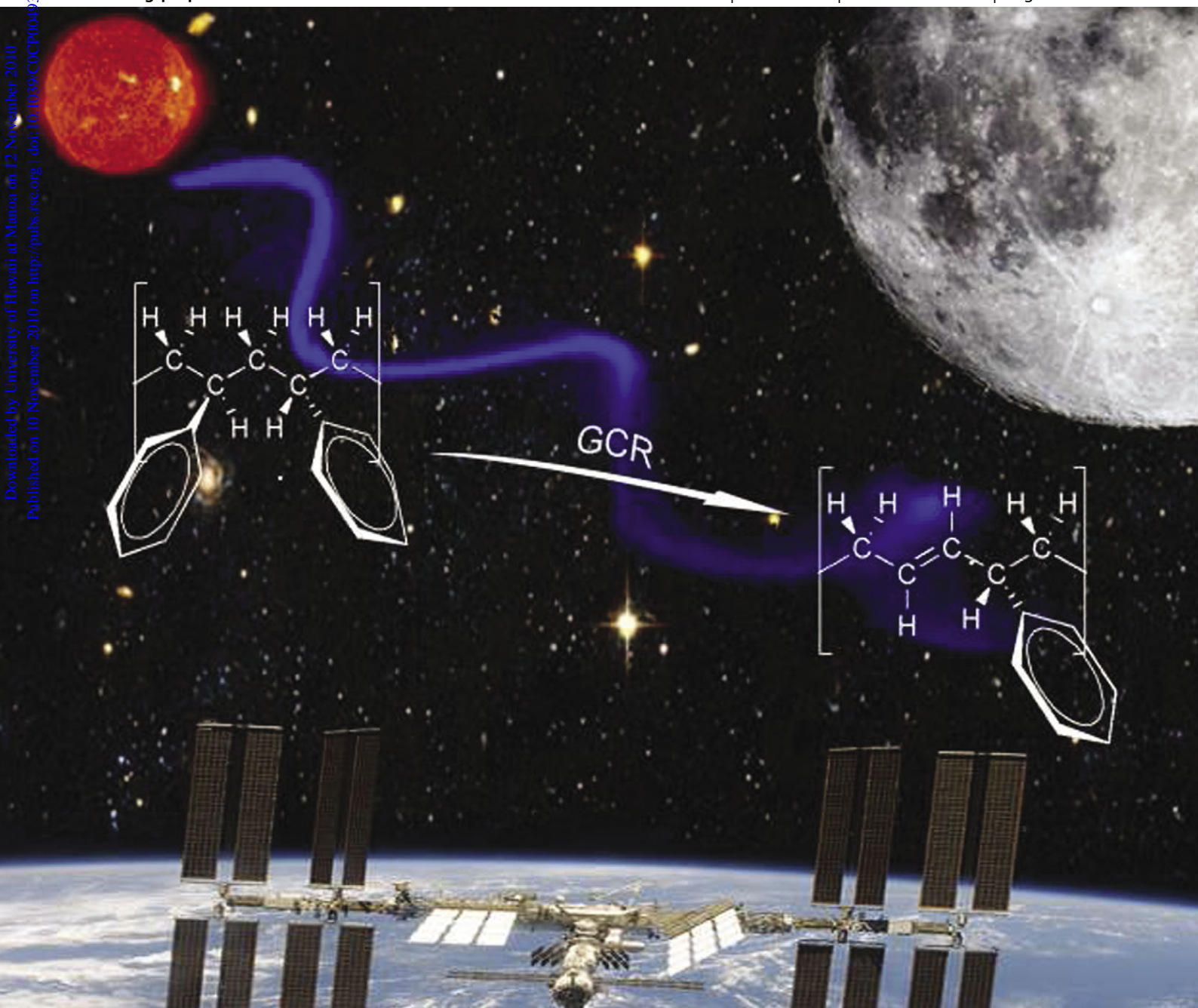
PCCP

Physical Chemistry Chemical Physics

www.rsc.org/pccp

Volume 12 | Number 45 | 7 December 2010 | Pages 14833–15148

Downloaded by University of Hawaii at Manoa on 12 November 2010
Published on 10 November 2010 on http://pubs.rsc.org | doi:10.1039/C0CP00493F



ISSN 1463-9076

COVER ARTICLE

Ennis and Kaiser
Mechanical studies on the
electron-induced degradation of
polymers

PERSPECTIVE

Fabiano and Pignataro
Engineering 3D ordered molecular thin
films by nanoscale control



1463-9076(2010)12:45;1-T

Mechanistical studies on the electron-induced degradation of polymers: polyethylene, polytetrafluoroethylene, and polystyrene

Courtney P. Ennis and Ralf I. Kaiser*

Received 9th May 2010, Accepted 31st August 2010

DOI: 10.1039/c0cp00493f

Mechanisms of the electron-induced degradation of three polymers utilized in aerospace applications (polyethylene (PE), polytetrafluoroethylene (PTFE), and polystyrene (PS)) were examined over a temperature range of 10 K to 300 K at ultra high vacuum conditions ($\sim 10^{-11}$ Torr). These processes simulate the interaction of secondary electrons generated in the track of galactic cosmic ray particles in the near-Earth space environment with polymer material. The chemical alterations at the macromolecular level were monitored on-line and *in situ* by Fourier-transform infrared spectroscopy and mass spectrometry. These data yielded important information on the temperature dependent kinetics on the formation of, for instance, *trans*-vinylene groups ($-\text{CH}=\text{CH}-$) in PE, benzene (C_6H_6) production in PS, fluorinated *trans*-vinylene ($-\text{CF}=\text{CF}-$) and terminal vinyl ($-\text{CF}=\text{CF}_2$) groups in PTFE together with molecular hydrogen release in PE and PS. Additional data on the radiation-induced development of unsaturated, conjugated bonds were collected *via* UV-vis spectroscopy. Temperature dependent *G*-values for *trans*-vinylene formation ($G(-\text{CH}=\text{CH}-) \approx 25\text{--}2.5 \times 10^{-4}$ units $(100 \text{ eV})^{-1}$ from 10–300 K) and molecular hydrogen evolution ($G(\text{H}_2) \approx 8\text{--}80 \times 10^{-5}$ molecules $(100 \text{ eV})^{-1}$ from 10–300 K) for irradiated PE were calculated to quantify the degree of polymer degradation following electron irradiation. These values are typically two to three orders of magnitude less than *G*-values previously published for the irradiation of polymers with energetic particles of higher mass.

Introduction

High-density polyethylene (HDPE; $(\text{C}_2\text{H}_4)_n$), polytetrafluoroethylene (PTFE; $(\text{C}_2\text{F}_4)_n$), and polystyrene (PS; $(\text{CH}_2\text{CH}(\text{C}_6\text{H}_5))_n$) (Fig. 1) are three prototype polymers, which are commonly utilized in spacecraft design and manufacture.¹ Adopted in their pure form or as monomeric constituents of copolymers such as PE/PTFE (Tefzel²), these low-weight materials with densities of $\rho(\text{HDPE}) = 0.94 \text{ g cm}^{-3}$, $\rho(\text{PS}) = 1.05 \text{ g cm}^{-3}$, and $\rho(\text{PTFE}) = 2.34 \text{ g cm}^{-3}$ possess important mechanical properties, such as toughness and resilience, that are sufficient for use in aeronautical applications. Therefore, in an effort to reduce spacecraft mass, polymers are often selected as a construction material for low-weight structures. Common aerospace applications for these polymers include—HDPE: radiation shields to protect astronauts from solar particle exposure,^{3,4} PTFE: incorporated in thermal control coatings on exterior surfaces,⁵ and PS: in low-density, general purpose thermal insulation materials.⁶ However, in the harsh low-Earth orbit (LEO) environment (150–1000 km⁷) and beyond in the interplanetary region of space, polymer surfaces interact with highly energetic particles emanating from the sun (solar wind) and from the Galactic Cosmic Radiation (GCR) field.⁸ These particles include ground and electronically excited atoms (for example atomic oxygen (AO) is the most abundant species in LEO at $\sim 10^8 \text{ atoms cm}^{-3}$)² and ions from the solar wind and GCRs.⁹ Polymer materials in these environments also experience ultra high vacuum (UHV)

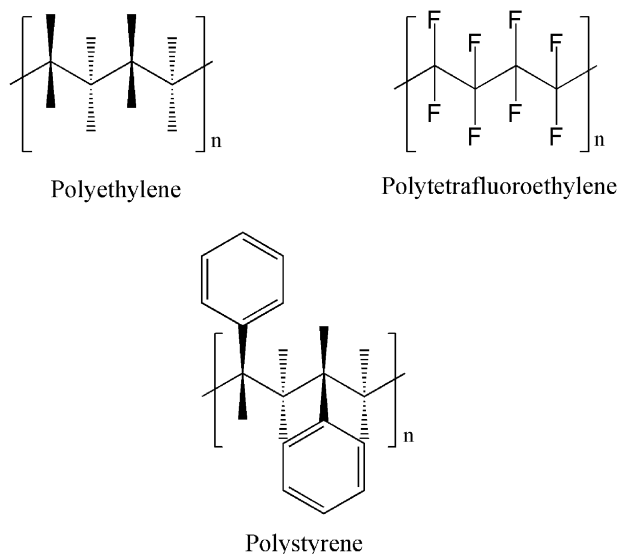
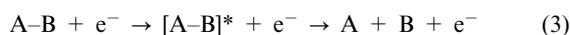
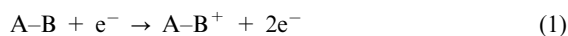


Fig. 1 Chemical structures displaying the repeating monomer units of polyethylene (PE), polytetrafluoroethylene (PTFE), and polystyrene (PS).

conditions (LEO: 10^{-9} – 10^{-11} Torr¹⁰) and extreme temperature fluctuations dependant on the position of the body to incident vacuum-ultraviolet/ultraviolet (VUV/UV: 100–400 nm) radiation from the Sun at a level of about 8% of the 1366 W m^{-2} solar constant.¹¹ The related temperature ranges are quite substantial; for instance, the exterior surfaces of the International Space Station experience temperature extremes of 123 and 423 K in its LEO orbit.¹²

Department of Chemistry, University of Hawai'i at Manoa, Honolulu, HI 96822, USA. E-mail: ralfk@hawaii.edu

In this context, it is important to note that GCRs consist predominantly of energetic, high-velocity protons (H^+ : 98%) and helium nuclei (He^{2+} : 2% *i.e.* α -particles) which intersperse almost isotropically throughout the interstellar medium.¹³ Possessing kinetic energies peaking at about 1 GeV in the Solar system, GCRs can penetrate organic matter easily and lose energy mainly by inelastic interaction with the target material; this generates a cascade of secondary electrons within the solid sample.^{14,15} These electrons also transfer their kinetic energy *via* inelastic scattering with the surrounding molecules, which can result in the breaking of chemical bonds and the generation of ionized species or radicals *via* ionization (eqn (1)), dissociative electron attachment involving a negative ion, $[A-B]^-$, by ‘attachment’ of the electron to an unoccupied molecular orbital (eqn (2)), and through unimolecular decomposition of internally excited molecules (eqn (3)).¹⁶ The branching ratio of reactions (1)–(3) and hence cross sections highly depend on the kinetic energy of the electrons.



In addition to GCRs entering the LEO, relativistic electrons¹⁷ are trapped by the Earth’s magnetic field, adding to the composition of damaging, energetic particles within the Van Allen radiation belts.¹³ Radiating out as two concentric tori parallel to the Earth’s equator, the Van Allen belts harbor relativistic electrons possessing energies to a maximum of about 5 MeV within the inner belt system (<2.4 Earth Radii (R_E)) and about 7 MeV in the outer belt system (2.8–12 R_E).¹³ Between the two belts, spacecraft and satellites are held in geosynchronous orbits, which experience low dosages of relativistic electrons. However, at times of intense solar wind activity¹⁸ the Van Allen belts can be compressed to expose these objects to high levels of irradiation (flux increase to about 10^4 electrons $cm^{-2} s^{-1} sr^{-1}$) at $R_E = 2.5$. Continuous irradiation of polymers by relativistic electrons can result in a process known as ‘deep dielectric charging’,⁹ where a large, localized charge build-up (several kV) in polymer insulation (*e.g.* coaxial cables) can culminate in an electric discharge event. Such events have been suspected to cause anomalies in the operation of sensitive electronic components.

The polyolefin polyethylene (PE) possesses a composition rich in hydrogen (carbon-to-hydrogen ratio of 1 : 2) and can be synthesized from ethylene by different methods. For example, free-radical polymerization is used to produce low-density PE (LDPE) resulting in a large degree of cross-linking between macromolecule chains, compared to the catalytic production of HDPE.¹⁹ HDPE possesses a lower degree of branching than LDPE compositions (LDPE < 0.941 $g\ cm^{-3}$), producing a higher tensile strength material due to stronger intermolecular bonding. Layers of HDPE are used as radiation shields lining the living quarters on the International Space Station⁴ to protect astronauts against high energy particle exposure.

The second polymer of interest, polystyrene (PS), also consists purely of carbon and hydrogen. However, due to the presence of a phenyl group as part of its repeating monomer unit, PS has shown to offer excellent resistance against radiation.²⁰ The phenyl ring effectively absorbs most of the energy from particle interaction with the polymer. After excitation, energy is thought to be efficiently dissipated through electronic transitions in the benzene ring back to the ground state.²¹ This effectively prevents the transfer of sufficient energy to initiate bond-breaking and polymer degradation processes. This is reflected in the low *G*-values (number of reactions or events promoted by 100 eV of absorbed energy)²⁰ previously determined for irradiated PS; in molecular hydrogen (H_2) production ($G(H_2) = 0.03$), in cross-linking yield ($G(X) = 0.05$) and in chain scission ($G(S) = 0.01$). These can be compared against the measured values for HDPE, ($G(H_2) = 3.0$, $G(X) = 1.0$ and $G(S) = 0.2$),²⁰ to demonstrate the high resistance of PS to polymer degradation processes initiated *via* irradiation.

Finally, polytetrafluoroethylene (PTFE), in contrast to PE and PS, is extremely sensitive to ionizing radiation and undergoes main chain scission as a preferential degradation process.²² The fluorine atoms in PTFE provide a steric hindrance; which exerts a large Coulombic repulsion force; this prevents the propagation of cross-links between chains.²⁰ In addition, the high dissociation energy associated with the carbon–fluorine bond ($452\ kJ\ mol^{-1}$)²¹ allows for the preferential breaking of the weaker C–C bonds in the macromolecule chain.²¹ This induces the production of radicals by scission processes along the polymer chain.

Due to the importance of these polymers in thermal coatings and as radiation shields, the interaction of ionizing radiation with PE, PS and PTFE has been studied extensively over the last decades by varying multiple experimental parameters; these are compiled in Table 1–3. In general, these studies covered a wide range of temperatures for PE (4–415 K), but were mainly performed at 273 K or above for PS and PTFE, while polymer radiation had been performed over a range of pressures from high vacuum (10^{-9} Torr) to ambient pressure. An array of ionizing particles (γ rays, e^- , H^+ , n) were used to irradiate the selected polymers, possessing energies from the keV range to 100 MeV orders of magnitude for high linear energy transfer (LET) collisions. For PE, molecular hydrogen (H_2) was observed to be the dominant gas phase product from multiple irradiation sources, leading to the detection of allyl and alkyl radicals along the PE chain. PS was observed to evolve H_2 , benzene (C_6H_6), methane (CH_4), and ethane (C_2H_6) fragments by mass spectrometric analysis, while alkyne and alkene radicals were inferred to be formed by irradiation processes. Most irradiation experiments for PTFE were conducted in oxidizing environments leading to the detection of Fourier-transform infrared (FTIR) signals derived from oxygen substituted absorption bands in the polymer. For all three polymers, identification of double bonds (*trans*-vinylene for PE and PS, and vinyl groups in PTFE) verified the unsaturated nature of the macromolecular chains by gas loss.

Even though previous studies have covered a wide range of temperature and pressure conditions, there is need for a

Table 1 Selected experimental studies concerning irradiation effects on polyethylene films

Reference	Thickness/nm	T/K	Pressure/Torr	Particle	Energy/eV	Products	Analytical method
Lawton <i>et al.</i> (1954) ⁴¹	3.05×10^6	298	'Vacuum'	e^-	—	H ₂ , CH ₄ -C ₁₁ H ₂₄	Thermistor gauge, MS
Williams and Dole (1959) ⁴⁸	5.08×10^4	298 and 415	'Vacuum'	⁶⁰ Co	—	H ₂ , vinylene	MS
Bodily and Dole (1966) ²⁷	8.00×10^4	77	760	γ -Ray ⁶⁰ Co	—	Polyene	UV-vis
Kang <i>et al.</i> (1967) ⁴⁹	2.67×10^5	298 and 393	'Vacuum'	γ -Ray ⁶⁰ Co	—	Vinylene	IR
Waterman and Dole (1970) ⁵⁰	2.67×10^5	77	'Vacuum'	γ -Ray e^-	1×10^6	Allyl, alkyl radicals	ESR, IR, UV-vis
Waterman and Dole (1971) ⁵¹	2.3×10^4 -2.6×10^5	4	'Vacuum'	e^-	1×10^6	Allyl radical, <i>trans</i> -vinylene	IR, UV-vis
Prošková <i>et al.</i> (2000) ⁵²	1.5×10^4	298	4×10^{-4}	Ar ⁺ Xe ⁺	6.3×10^4 1.56×10^5	Vinylene	ESR, UV-vis
Zeid <i>et al.</i> (2000) ⁵³	1.0, 1.5, 2.2 $\times 10^4$	298	760	e^- n	1.5×10^6 thermal	<i>trans</i> -Vinylene	FTIR, FT-Raman, UV-vis
Kondyurin <i>et al.</i> (2002) ⁵⁴	5.0×10^4	<313	10^{-3}	N ⁺	2.0×10^4	Vinylene, carbonyl groups	IR-ATR, UV-vis
Mélot <i>et al.</i> (2003) ⁴²	2.8×10^4	8 and 290	'Vacuum'	¹⁶ O ⁺ ³² S ⁺	13.6×10^6 11.2×10^6	Vinyl, alkyne and allene groups	FTIR
Makkonen-Craig <i>et al.</i> (2005) ⁵⁵	5.0×10^4	298	760	H ⁺	9.4×10^6	<i>trans</i> -Vinylene	UV-vis
Ali (2007) ⁵⁶	$4.0-5.0 \times 10^5$	298	—	e^-	1.5×10^6	Allyl radical	ESR, FTIR
Singh <i>et al.</i> (2007) ⁵⁷	1.00×10^5	298	4×10^{-6}	H ⁺ ⁶⁴ Cu ⁺	3×10^6 120×10^6	<i>trans</i> -Vinylene	IR, UV-vis, XRD

Table 2 Selected experimental studies concerning irradiation effects on polystyrene films

Reference	Thickness/nm	T/K	Pressure/Torr	Particle	Energy/eV	Products	Analytical method
Švorčík <i>et al.</i> (1997) ⁴⁴	1.00×10^6	298	760	e^-	14.89×10^6	Conjugation, oxidation	UV-vis, FTIR
Martínez-Pardo <i>et al.</i> (1998) ⁵⁸	$4.0-6.0 \times 10^4$	298	'Vacuum'	H ⁺	$1.0-1.8 \times 10^6$	<i>trans</i> -Vinylene, conjugation	UV-vis, FTIR
Makkonen-Craig <i>et al.</i> (2005) ⁵⁵	5.5×10^4	298	760	H ⁺	9.4×10^6	Conjugation, unsaturation	UV-vis
Ferry <i>et al.</i> (2008) ⁴⁵	—	298	'Vacuum' or He atm	e^- C O Ar	1.00×10^6 11.04×10^6 11.04×10^6 6.3×10^6	<i>trans</i> -Vinylene, alkyne and alkene C ₆ H ₆ gas evolution	FTIR
Massey <i>et al.</i> (2008) ⁵⁹	15 ± 5	300	10^{-9}	e^-	<100	H ₂ , CH ₃ ⁺ , C ₂ H ₃ ⁺ , C ₂ H ₅ ⁺ , C ₃ H ₅ ⁺	MS
Singh and Samra (2008) ³⁷	1.25×10^5	298	4×10^{-6}	H ⁺	3×10^6	Conjugation, unsaturation, oxidation	UV-vis, FTIR
Singh <i>et al.</i> (2008) ⁶⁰	1.25×10^5	298	10^{-6}	⁵⁸ Ni ⁷⁺	8.6×10^7	Alkyne	UV-vis, FTIR

Table 3 Selected experimental studies concerning irradiation effects on polytetrafluoroethylene (PTFE) films

Reference	Thickness/nm	T/K	Pressure/Torr	Particle	Energy/eV	Products	Analytical method
Fischer <i>et al.</i> (1998) ⁶¹	5.00×10^4	298	760	e^-	1.0×10^6	Oxidation products, <i>i.e.</i> -COF, -COOH	FTIR
Tian and Xue (1998) ⁶²	$0.5-1.0 \times 10^4$	298	760	⁶⁰ Co	—	Hydration, <i>i.e.</i> C-H	FTIR
Lappan <i>et al.</i> (1999) ²²	5.00×10^5	298 and 638	7.5×10^{-4}	γ -Ray e^-	1.5×10^6	oxidation products, <i>i.e.</i> -OH, -COOH Conjugation, -CF ₃ branches	FTIR
Peng <i>et al.</i> (2003) ⁶³	5.00×10^4	<313	7.5×10^{-6}	H ⁺	$0.6-1.7 \times 10^5$	Conjugation, -CF ₃ branches, C/F substitution	UV-vis, FTIR
Kumar <i>et al.</i> (2008) ⁶⁴	8.0×10^4	298	4×10^{-6}	Si ⁸⁺	1.0×10^8	Conjugation	UV-vis

detailed investigation into the degradation processes of PE, PTFE and PS when exposed to electrons of the energies observed in LEO and near-Earth environments. These investigations will cover for the first time a systematic investigation of all three polymers under identical experimental conditions at UHV (8.0×10^{-11} Torr) pressures in a simulation chamber, over a wide range of temperatures from 10 K to 300 K. This effectively replicates a range of space environments, from the high temperatures of surfaces exposed

to solar radiation, to the cold surfaces like the shadowed side of the moon. In addition, the authors will irradiate the polymer samples with 5 keV electrons, simulating the effect of high energy (few keV) secondary electrons, which are typically generated in a polymer after exposure to energetic GCR particles in LEO and the interplanetary environment. Further, the analysis will be conducted on-line and *in situ*, quantitatively monitoring the solid state *via* FTIR spectroscopy and the gas phase *via* mass spectrometry.

Experimental

Polymer film samples of HDPE (0.01 mm), PTFE (0.005 mm) and PS (0.025 mm) were obtained from Goodfellow Corporation. The samples were mounted onto a highly polished silver substrate with a facial area of 31.75×31.75 mm. The silver substrate was attached to the freely rotating cold-head of a closed cycle helium refrigerator (CTI-Cryogenics CP-1020). This cold head was enclosed in an UHV chamber that was evacuated down to 5×10^{-11} Torr using an oil-free magnetically suspended turbo pump in series with an oil-free backing scroll pump. At these conditions, the temperature of the cold head could reach 11.3 ± 0.5 K. The temperature was measured by a silicon diode connected to a Lakeshore 331 temperature controller; the latter maintained sample temperatures of 11.3 K, 100 K, 200 K, and 300 K. The polymer films were then irradiated with 5 keV electrons supplied by an electron gun (SPECS EQ 22) for 3 h at beam currents between 100 and 1000 nA. The manufacturer states an electron extraction efficiency of 78.8%. The scanning area incident to the sample surface was 3.2 ± 0.5 cm².

The analysis of the irradiated polymer films was first performed with a Nicolet 6700 FTIR spectrometer operating in absorption–reflection–absorption mode at a 75° angle-of-incidence to the film surface on-line and *in situ* during the irradiation exposure. Spectra were recorded over the near-infrared (NIR) and mid-infrared (mid-IR) ranges (10 000–2000 and 4000–400 cm⁻¹) utilizing a white-light and infrared light source for the two respective regions and a mercury–cadmium–telluride detector cooled with liquid nitrogen. The IR spectra were recorded at a resolution of 2 cm⁻¹, with each spectrum being collected from 196 individual scans integrated over 2.5 min. Gaseous species produced *via* the electron irradiation were recorded by a Balzer QMG 420 quadrupole mass spectrometer (QMS) operating in residual gas analyzer mode. Typically, each sample was cooled to the desired temperature for the irradiation procedure then, upon completion, left for 30 min to allow for gas diffusion and chain re-organization processes to stabilize. The sample was then heated to 300 K by a controlled heating program at a rate of 0.5 K min⁻¹ to allow for the analysis of volatile products as they sublimed from the target. After heating to 300 K, the polymer films were removed from the UHV chamber for analysis with a Thermo Scientific Evolution 300 UV-vis spectrometer. Samples were mounted and measured at room temperature in both transmission and reflection modes. Spectra were recorded over a spectral range of 190–1100 nm at a resolution of 1 nm.

Results

Irradiation conditions

Electron penetration. To evaluate the radiation effects quantitatively, it is important to compute the electron penetration depths inside the polymers and also the energy transferred from the electrons to the polymer samples. The penetration depths of the electrons were calculated using the CASINO Monte Carlo program;²³ the results are compiled in Table 4. This program simulates the transfer of kinetic energy

Table 4 Electron penetration depths and dosages

	Density/ g cm ⁻³	Electron penetration depth/nm	Electron emission current/nA	Dosage/ eV monomer unit ⁻¹
PE	0.94	750 ± 5	1000	175 ± 30
PTFE	2.2	400 ± 3	100	50.1 ± 8.5
PS	1.05	680 ± 4	1000	643 ± 109

from the impinging electrons to the polymer material with known density and chemical composition; penetration depths are calculated and averaged over 100 000 trajectories. These calculations suggest that the electrons only penetrate less than 1 μm of the sample. Therefore, only the polymeric chains at the surface of the material are exposed to the maximum energy possessed by the irradiating electrons. Consequently, it is this surface region of a polymer film sample that is expected to generate degradation products from interaction with energetic electrons that will be analytically observed during the present study.

Electron dosage. Calculations were performed to determine the *average* energy supplied to each monomer subunit of the irradiated polymers during the 3 hour electron irradiation period. Firstly, the volume of polymer sample exposed to the incident electron beam is calculated by the product of the irradiation area, A (3.2 cm²), and the electron penetration depth, d , for a specific polymer (Table 4). Subsequently, the total number of monomer units ($\sum(\text{monomer})$) exposed to the electron irradiation was calculated (eqn (4)). Here, ρ is the density of the polymer, N_a is Avogadro's number, and M_m is the molecular mass of the monomer unit.

$$\sum_{\text{monomer}} = A \times d \times \rho \times N_a / M_m \quad (4)$$

The total energy E provided by the electron irradiation is then calculated *via* eqn (5), where I is the emission current of the electron gun, E_{kin} is the electron energy (5 keV), F is the electron extraction efficiency of the source ($F = 0.788$), t is the irradiation time (1.08×10^4 s), and e is the elementary charge (1.60×10^{-19} C).

$$E(e^-) = I \times E_{\text{kin}} \times F \times t / e \quad (5)$$

Eqn (4) and (5) are then combined to calculate the average dose absorbed by each monomer unit of the polymer (eqn (6)). These values, in units of eV monomer unit⁻¹, can be viewed in Table 4. These data alone suggest energy absorptions of up to 643 eV per monomer unit; to place this into context, typical carbon–hydrogen bonds are up to 4.5 eV strong. Therefore, the averaged dose absorbed per monomer unit has the potential to induce substantial damage to the polymer samples.

$$\text{Dose} = E(e^-) / \sum_{\text{monomer}} \quad (6)$$

Polyethylene

Physical structure. PE possesses the simplest chemical structure of all polymers and should therefore produce a relatively simple IR spectrum. Krimm *et al.*²⁴ compiled the symmetry elements associated with a pair of PE monomer units in a single chain ((C₂H₄)₂) calculating a total of 14

normal modes of vibration of which five were identified as being IR active. However, a number of different factors combine to complicate IR spectra collected from pristine PE (Fig. 2, Table 5). PE samples contain disparate regions of crystalline (50–85%) and amorphous microstructures.²⁵ Both chain configurations in the bulk environment induce distinct degrees of perturbation to the normal modes of vibration of the repeating PE monomer unit, resulting in small absorption band shifts in the IR spectrum from their theoretical positions. In addition, due to their manufacture by extrusion or cold-drawing processes, PE films display an anisotropic macromolecule chain orientation in the direction of the applied stretching.²⁵ For this reason, the covalent bonds within the PE monomer units vibrate either perpendicular or parallel to the chain axis, allowing for the fundamentals to be further categorized due to their polarization to the incident IR beam. This effect leads to absorption bands displaying intensities correlating to the incident beam direction and

polarization, in relation to the position of an orientated PE film sample. However, for the present set of experiments, where the incoming unpolarized IR beam is perpendicular to the chain orientation of the PE film, the polarization effect of absorption features in the recorded spectra is diminished. At a perpendicular angle-of-incidence, the normal modes vibrating parallel to the polymer chain axis absorb a similar amount of radiation to the normal modes vibrating perpendicular to the chain axis. Finally, deviating from theoretical models, the PE chain lengths are not of infinite length, meaning terminal $-\text{CH}_3$ groups possess their own specific modes of vibration in the PE spectra. It is often observed that the positions of the $-\text{CH}_3$ end group absorption bands are only slightly shifted from the corresponding fundamentals of the repeating $-\text{CH}_2-$ units, which can complicate the assignment of some peaks.

Infrared spectroscopy. Fig. 2 (top, left) displays the baseline corrected mid-IR region for PE film at 10 K recorded during

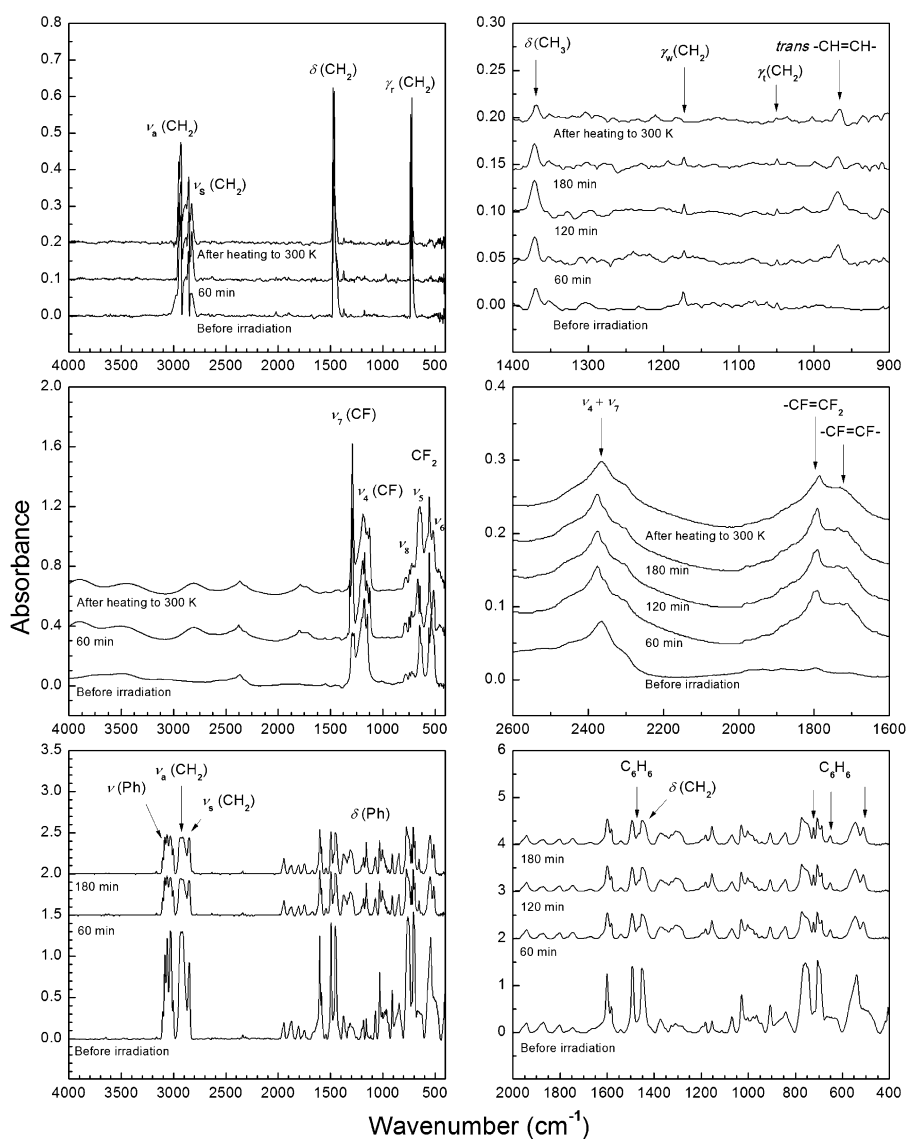


Fig. 2 Mid-infrared spectra of 10 K PE film (top); 10 K PTFE film (middle) and 300 K PS film (bottom). All films are irradiated with 5 keV electrons for 3 hours. The samples at 10 K are then heated at a rate of 0.5 K min^{-1} to 300 K.

Table 5 Vibrational assignments of polyethylene (PE)

Absorption/cm ⁻¹	Irradiation absorption/cm ⁻¹	Literature value ^a /cm ⁻¹	Assignment ^a	Characterization
735, 720	968	734, 721	$\gamma_r(B_{1u}, B_{2u})$	CH ₂ rock
		965 ^b	$-\text{CH}=\text{CH}-$	<i>trans</i> -Vinylene
1050		1050	$\gamma_t(B_{3u})$	CH ₂ twist
1173		1175	$\gamma_w(B_{3u})$	CH ₂ wag
1370		1369	δ	CH ₃ bend
1473, 1462		1473, 1463	$\delta(B_{1u}, B_{2u})$	CH ₂ bend
1897		1890	$\gamma_r + \gamma_t$	Overtone
2018		2010 ^c	$\gamma_w + \gamma_r$	Overtone
2824		—	—	Overtone (?)
2850		2851	ν_s	CH ₂ symmetric stretch
2926		2919	ν_a	CH ₂ asymmetric stretch
2950		2959	ν_a	CH ₃ asymmetric stretch

^a Bower and Maddams (1989).²⁵ ^b Abdel-Fattah *et al.* (1998).²⁶ ^c Krimm *et al.* (1956).²⁴

the present reflection FTIR experiments. Spectra are shown for the pristine sample, after 1 hour of the irradiation, and after the irradiated sample was heated to 300 K. Averaged peak positions for the PE fundamental vibration modes are summarized in Table 5, together with the peak positions and assignments identified in the literature.²⁴ Electron irradiation experiments were also conducted at 100, 200, and 300 K. However, the recorded spectra were similar to those produced for the 10 K investigations. Therefore, these spectra are not presented for discussion, as the results produced for the 10 K experiments can be considered also to apply for the high temperature studies. The two intense absorption regions previously assigned to the γ_r $-\text{CH}_2$ rocking fundamental (735 and 720 cm⁻¹) and the δ_a $-\text{CH}_2$ bending fundamental (1473 and 1462 cm⁻¹) are clearly identified in all spectra. These fundamental modes appear as doublets due to correlation splitting associated with inter-chain interactions in the crystalline regions of PE, resulting in the identification of the B_{1u} (higher frequency) and the B_{2u} (lower frequency) species for each normal mode.²⁵ At higher frequency regions of the spectra, the ν_s $-\text{CH}_2$ symmetric stretching fundamental (2850 cm⁻¹) and the ν_a $-\text{CH}_2$ asymmetric stretching fundamental (2926 cm⁻¹) are also observed to correspond well with the literature²⁴ in all recorded spectra. In addition, the ν_a $-\text{CH}_3$ asymmetric stretching absorption band (2950 cm⁻¹), associated with the $-\text{CH}_3$ terminal groups of the PE chain or side-branches, is also identified in the spectra. However, no absorption band is identified for the ν_a $-\text{CH}_3$ asymmetric stretching mode at the theoretical 2874 cm⁻¹ position. This is probably due to the absorption band being previously calculated²⁴ as weak in intensity and due to being positioned between the strong absorbance features assigned to the C–H stretches of the $-\text{CH}_2$ repeating unit.

Fig. 2 (top, right) shows the PE film spectra collected at 1 hour intervals of irradiation in the 1400–900 cm⁻¹ mid-IR region, as well as the spectrum recorded after the PE film was heated from 10 to 300 K following electron irradiation. The γ_w CH₂ wagging fundamental can now be identified in this region at 1173 cm⁻¹, together with the very weak γ_t CH₂ twisting fundamental at 1050 cm⁻¹, both of which are in good agreement with the literature.²⁴ The irradiation of the PE sample with 5 keV electrons produces a new absorption band positioned at 968 cm⁻¹. This absorption feature is observed

to increase in absorption intensity during 2 hours of irradiation before leveling off at an intensity of about 0.02 during the final hour of irradiation. The absorption band retains its intensity during the controlled heating of the sample from 10–300 K. The 968 cm⁻¹ absorption band can confidently be assigned to the formation of the *trans*-vinylene ($-\text{CH}=\text{CH}-$) group.²⁶ This absorption band is the only new feature observed in the mid-IR spectra for electron irradiated PE and is also identified in the spectra obtained from PE samples irradiated at 100, 200, and 300 K. The presence of the *trans*-vinylene peak suggests an unsaturation of the PE chain via irradiation-induced hydrogen loss. This process will be discussed in further detail in the Discussion.

Mass spectrometry. For the experiments involving the electron irradiation of PE films at 10, 100, 200, and 300 K sample temperatures, only molecular hydrogen (H_2^+ : $m/z = 2$) and atomic hydrogen (H^+ : $m/z = 1$) displayed an increase in their detectable ion-current during the 3 hour irradiation period. No higher masses pertaining to alkanes $\text{C}_x\text{H}_{2x+2}$ ($x = 1-14$), or their associated fragment species appeared to be generated by the breakdown of PE. Fig. 3 (top) displays the ion profile for H_2^+ during the 3 hour radiation period over the various sample temperature experiments. Generally, the peak current occurs immediately after the onset of the electron exposure ($t = 0$ min) for the higher sample temperature experiments (100–300 K) before displaying an exponential-like decay over time. The current is then observed to drop to the background level of the blank experiment after completion of the irradiation ($t = 180$ min). The peak current displays a strong correlation to the temperature of the irradiated PE sample. At 300 K, the peak ion current is measured to be 1.35×10^{-10} A, an order of magnitude higher than the 1.40×10^{-11} A peak current recorded at 200 K. However, this pattern is not upheld for the mass spectrum recorded for the 10 K experiment. The peak current is not observed to correspond with the initiation of irradiation, but slowly increases to a maximum of 5×10^{-13} A above its baseline level at about 2 hours after first electron exposure. At 250 min, after the commencement of controlled heating at 0.5 K min⁻¹ and corresponding to a sample temperature of 20 K, the ion current is observed to sharply increase to 6.0×10^{-12} A as sublimation of the hydrogen from the PE sample is initiated.

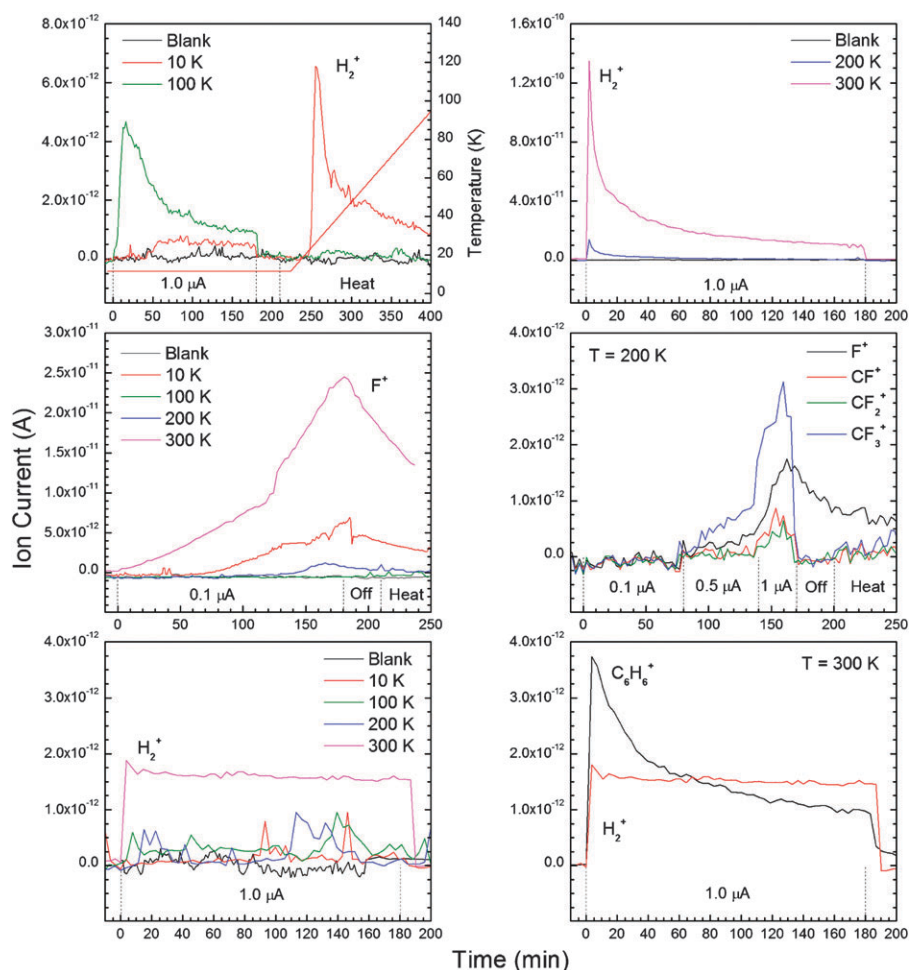


Fig. 3 Mass spectra of PE film (top); PTFE film (middle) and PS film (bottom). All films are irradiated with 5 keV electrons for 3 hours. Blank spectra of pristine polymer films are also provided. Gas phase species evolved during electron irradiation, which were detected by QMS, are indicated in the spectra for each polymer.

As the PE temperature increases, the ion current is further observed to decrease in a similar decay pattern as previously seen for the higher sample temperature experiments.

UV-vis spectroscopy. Fig. 4 (top) displays the transmission UV-vis spectra recorded for the series of irradiation experiments performed on PE films. An additional spectrum of a PE film not exposed to electron irradiation is included for comparison. For the pristine PE sample, the far UV limit of the spectra (<250 nm) displays a strong absorbance edge produced by $\sigma\text{-}\sigma^*$ transitions, associated with both the C–H and C–C chromophores that feature in the PE composition. However, the edge of this absorbance characteristic is observed to be red-shifted to longer wavelengths after the electron irradiation. The magnitude of the shift correlates with an increase of the sample temperature during exposure. This red-shift appears to overlap into the visible region (>400 nm), where visual investigation of the irradiated films reveals a consistent yellow color covering the square irradiation area. A shoulder can also be observed to arise from the irradiation experiments in the 220–260 nm range. If taken to center at 236 nm, the shoulder can be assigned to the $\text{C}=\text{C}$ diene group undergoing a transition from the ground 1A_g state to the

higher 1B_u electronic state.²⁷ An increase in the density of the conjugated double bonds within the polymer structure accounts for the increase in UV absorbance, observed as the temperature of the PE sample is increased from 10 K to 300 K. This is probably a result of the enhanced ability of mobile hydrogen atoms generated during the electron irradiation to diffuse more efficiently through the polymer microstructure at higher temperatures.²⁸ This process would also prevent the reactive hydrogen atoms from back-reacting with the newly formed $\text{C}=\text{C}$ sites.

Polytetrafluoroethylene

Physical structure. PTFE chains can exist as a number of different structural conformers dependent on the temperature of the material.²⁹ At low temperatures, PTFE forms helical structures coiled about the axis of the carbon chain. Due to the non-linear twist displayed between neighboring monomer units, the investigation of helical PTFE point groups and their associated symmetry species are complex for these conformers. However, comprehensive studies of the proposed helical structures have been reported in the literature,³⁰ together with the calculated vibrational frequencies of the fundamentals and also their activity for IR analysis. At 292 K, PTFE films

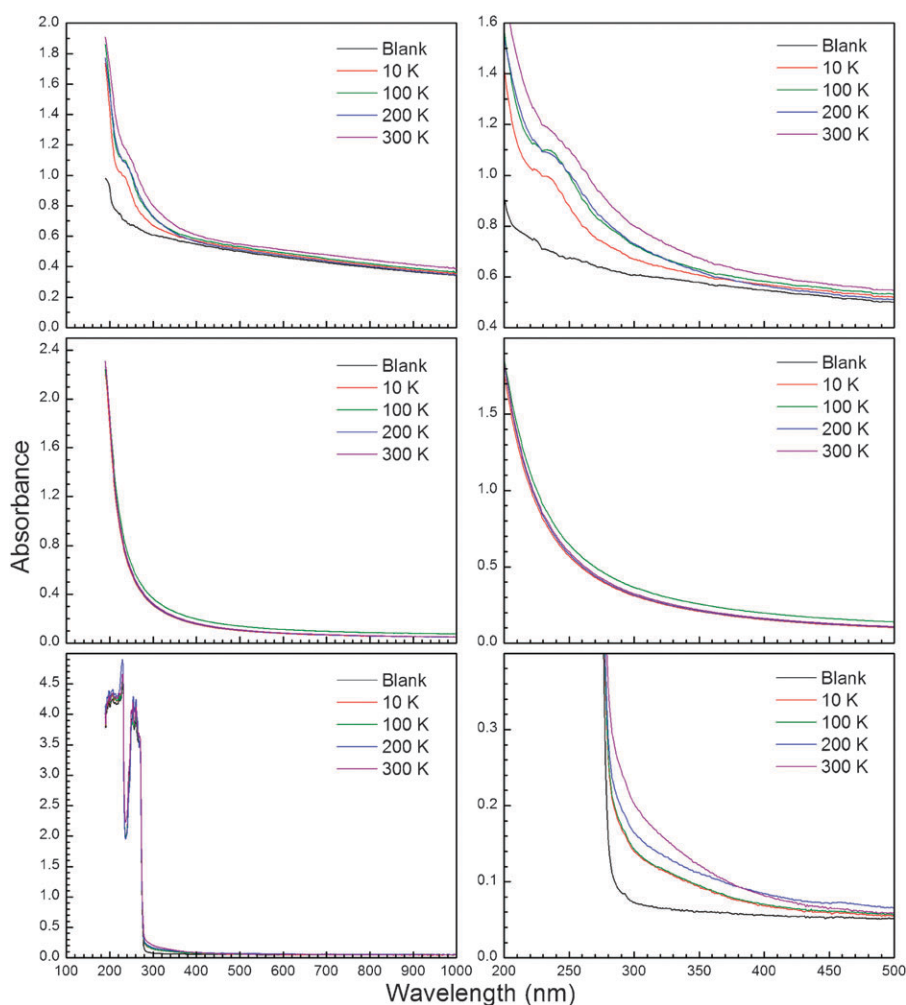


Fig. 4 UV-visible spectra of PE film (top); PTFE film (middle) and PS film (bottom). All films are irradiated with 5 keV electrons for 3 hours at sample temperatures of 10, 100, 200 and 300 K. Blank spectra of pristine polymer films are also included.

undergo a conformation transition to a planar structure,³¹ with the calculated normal vibration modes changing as a consequence. In addition, the different structures of PTFE chains are observed to be distributed between ordered and amorphous regions. The degree of order for the bulk polymer has also been correlated to the temperature of the sample and also to the physical form of material analyzed (*i.e.* powder, film). Increased structural order has been observed with PTFE powders and suspensions, while commercial PTFE films, formed from techniques involving heating the material to above its softening point (600 K),³¹ display a more amorphous microstructure, which is retained after cooling. In respect to FTIR analysis of PTFE samples, the normal vibrations of the $-\text{CF}_2$ subunits induce large oscillations in the dipole moment of the internal covalent bonds. It can be expected that these normal modes will interact strongly with incident IR radiation to produce intense absorption bands in the experimental spectra.

Infrared spectroscopy. Fig. 2 (middle, left) displays the 4000–400 cm^{-1} mid-IR region for PTFE film recorded during the present experiments at 10 K. The thinner PTFE film

samples (5 μm) did not produce severe interference patterns in the experimental spectra, meaning baseline correction procedures are avoided. It has been postulated in the literature³¹ that the position of the absorption bands associated with the PTFE $-\text{CF}_2$ stretching fundamentals, located in the 1350–1100 cm^{-1} frequency range, are dependent on the temperature of the sample. At 10 K, the peaks are usually blue-shifted to higher frequencies, due to an alteration in the geometry of the helical structure. However, the frequency shifts associated with temperature change do not appear to be uniform between different $-\text{CF}_2$ stretching peaks, making the assignment of fundamentals identified in the current experimental spectra difficult, particularly when comparing to those made previously in the literature, which were collected at different sample temperatures. Therefore, the 10 K absorption bands observed in Fig. 2 for the pristine PTFE sample can be best compared with literature values collected at 83 K.³¹ Using these literature values compiled in Table 6, the peak at 1287 cm^{-1} can be assigned to the $\nu_7(\text{E}_1)$ $-\text{CF}_2$ asymmetric stretching mode, while the broad, overlapping features at 1176 and 1146 cm^{-1} can be cautiously assigned to the $\nu_7(\text{A}_2)$ $-\text{CF}_2$ asymmetric stretching fundamental and the $\nu_4(\text{E}_1)$ $-\text{CF}_2$

Table 6 Vibrational assignments of polytetrafluoroethylene (PTFE)

Absorption/cm ⁻¹	Irradiation absorption/cm ⁻¹	Literature value ^a /cm ⁻¹	Assignment ^c	Characterization
511		516	$\nu_6(A_2)$	$\gamma_r(CF_2)$
553		553	$\nu_5(E_1)$	$\delta(CF_2)$
642		638	$\nu_8(A_2)$	$\gamma_w(CH_2)$
	663	—	—	Amorphous
725		718	—	Amorphous
746		738	—	Amorphous
782		778	—	Amorphous
	1123	—	—	Amorphous
1146		1152 ^b	$\nu_4(E_1)$	–CF ₂ symmetric stretch
	1172	—	$\nu_4(E_1)$	–CF ₂ symmetric stretch
1176		1213 ^b	$\nu_7(A_2)$	–CF ₂ asymmetric stretch
	1185	—	—	—
1287		1298 ^b	$\nu_7(E_1)$	–CF ₂ asymmetric stretch
	1311	—	$\nu_7(E_1)$	–CF ₂ asymmetric stretch
	1735	—	–CF=CF–	Chain C=C
	1791	—	–CF=CF ₂	Terminal C=C
2375		2367	$\nu_4(E_1) + \nu_4(A_2)$	Combination

^a Moynihan (1959).²⁹ ^b Masetti *et al.* (1973).³¹ ^c Liang and Krimm (1956).³⁰

symmetric stretching fundamental respectively. At lower frequencies, the –CF₂ fundamentals appear to be less sensitive to temperature, resulting in band assignments that are more consistent with the literature. These are the $\nu_6(A_2)$ –CF₂ rocking mode at 511 cm⁻¹, the $\nu_5(E_1)$ –CF₂ bending mode at 553 cm⁻¹ and the $\nu_8(A_2)$ –CF₂ wagging mode at 642 cm⁻¹. Also identified in the 10 K pristine PTFE spectrum are a series of ill-defined bands in the region between 780–720 cm⁻¹. These are thought to derive from the amorphous regions of the material²⁹ where rotational conformers about the C–C axis give rise to absorbance features attributed to *trans* and *gauche* configurations.

Recorded at $t = 60$ minutes after the onset of irradiation in Fig. 2 (middle, left), a considerable alteration to the absorption spectrum over the full 1600–400 cm⁻¹ PTFE mid-IR spectral range is observed when compared to the pristine 10 K spectrum. New absorption bands are identified at 1311, 1185, 1123 and 663 cm⁻¹. However, these peaks surround the local regions of the previously identified PTFE fundamentals from the pristine sample and do not display any increase in intensity with increased irradiation time, rather they appeared in the spectra recorded immediately following electron exposure. For this reason the new absorption bands are not considered to be derived from chemical alteration of the PTFE material. Instead it is proposed that these new absorption features are a consequence of a chain reorientation induced by energetic electron exposure, perhaps relaxing the low temperature helical conformation in the more ordered regions. This would result in the splitting of the PTFE fundamentals evident in the spectra (*i.e.* the 1311 and 1287 cm⁻¹ modes for the $\nu_7(E_1)$ –CF₂ asymmetric stretch) originating from the two chain structures.

However, at the higher frequency 1800–1700 cm⁻¹ mid-IR region, depicted in Fig. 2 (middle, right), a broad absorption feature is identified that displays intensity dependence on the time of electron exposure. This is displayed in the spectra recorded for 10 K PTFE films after exposure to 5 keV electrons at a current of 0.1 μ A, over subsequent 1 hour irradiation periods. After reaching its maximum absorbance

of about 0.75 over 3 hours of electron irradiation, the band, with a defined peak at 1792 cm⁻¹, does appear to diminish slightly in intensity after the sample is heated back to 300 K. Assignment of absorption peaks to unsaturated –CF=CF– (1740 cm⁻¹) centers and the terminal –CF=CF₂ (1795 cm⁻¹) groups have been previously made in the literature²² after exposure to 1.5 MeV electron irradiation at room temperature. These assignments should carry through to the absorption bands observed in the same region for the present experiments, with their broader appearance probably due to the structural diversity of PTFE films at 10 K. Finally, after controlled heating of the irradiated sample to 300 K, it is observed that the absorption bands formed by the splitting effect in the 1600–400 cm⁻¹ region (1311, 1185 and 663 cm⁻¹), first observed for the 10 K irradiation, have disappeared. This effect can be attributed to a known²⁹ PTFE phase change from the helical conformation to the planar conformation at 292 K, promoting the normal modes associated with a more amorphous chain distribution.

Mass spectrometry. Depicted in Fig. 3 (middle, left), the QMS analysis of PTFE samples irradiated with 5 keV electrons resulted in the detection of fluorine (F) atoms (F⁺: $m/z = 19$). In contrast to the immediate increase of molecular hydrogen upon the commencement of irradiation in the PE mass spectra discussed previously, the emergence of fluorine atoms from the irradiated PTFE samples is gradual, with the recorded ion counts for the species increasing steadily over the 3 hour irradiation period. In addition, all mass spectra displaying a gradual increase in fluorine production over irradiation time did not display a sudden decrease in the fluorine ion current back to the background level after electron exposure, as seen in the mass spectra of irradiated PE samples for gaseous molecular hydrogen. In contrast, it is observed in the PTFE mass spectra that the ion current for F⁺ decreased steadily after the completion of irradiation back to the baseline level. These findings suggest a slower diffusion processes applied to fluorine atoms from the subsurface of the irradiated PTFE film to the surface interface, in comparison to the

spatially smaller molecular hydrogen released from irradiated PE. Likewise, we shall stress that we did not observe molecular fluorine (F_2^+), possibly due to the limited recombination of fluorine atoms to form molecular fluorine.

The PTFE samples at 10 and 100 K irradiated with an electron emission current of 0.1 μA did not show any increase in ion current above the background levels, either during irradiation or during subsequent controlled heating of the sample to 300 K. In this respect a correlation between the maximum ion current and the temperature of the irradiated PTFE film can be drawn. The 300 K sample possessed a peak fluorine ion current of 2.4×10^{-11} A at the end of the irradiation period ($t = 180$ min) while after the same irradiation period, the 200 K sample recorded a peak ion current of 1.0×10^{-12} A. Due to the absence of any detectable increase in the fluorine ion count for the 10 K PTFE sample irradiated with an electron emission current of 0.1 μA , a subsequent mass spectrum is recorded for a similar 10 K experiment with an increased emission current of 1.0 μA . These experimental conditions produced a peak fluorine current of 7.0×10^{-12} A, implying that electron emission current may have a more profound effect on the release of fluorine from irradiated PTFE than the sample temperature.

To investigate this further, an experiment involved irradiating a 200 K PTFE film with 5 keV electrons at increasing emission currents of 0.1 μA ($t = 0$ –80 min), 0.5 μA ($t = 80$ –140 min) and finally 1.0 μA ($t = 140$ –170 min). The spectra recorded for these experiments can be investigated in Fig. 3 (middle, right). In addition to the previously identified atomic fluorine signal, the species CF^+ ($m/z = 31$), CF_2^+ ($m/z = 50$) and CF_3^+ ($m/z = 69$) are recorded in the mass spectra. F and CF_3 are not detected above their baseline signal until the emission current is increased to 0.5 μA , where a gradual increase in ion current for these species is observed during the hour long irradiation. For the final 30 minutes of irradiation, where the emission current is increased to 1.0 μA , the ion signals for F, CF, CF_2 and CF_3 increased rapidly with CF_3 appearing to generate the highest ion current of 2.6×10^{-12} A. After completion of the irradiation period ($t = 170$ min) the ion currents for CF, CF_2 and CF_3 immediately returned to the baseline level, while the ion current for F displayed a similar gradual decrease to that observed in the previous irradiated PTFE mass spectra. This observation provides further evidence for the slow diffusion of F atoms through the PTFE microstructure. The temporal evolution of the ions of CF and CF_2 suggest that these are actually formed *via* dissociative ionization of the CF_3 species since the profiles of the lower masses overlap with those from CF_3 .

UV-vis spectroscopy. The transmission UV-vis spectra collected after the 3 hour irradiation of PTFE films with 5 keV (0.1 μA) electrons at sample temperatures of 10, 100, 200, and 300 K are shown in Fig. 4 (middle). Also displayed is the spectrum for a PTFE film which had not been exposed to electron irradiation. The increase in UV absorption at wavelengths lower than 300 nm is due to σ – σ^* transitions associated with the C–C backbone of the PTFE macromolecule. It is clearly observed over the entire experimental UV-vis range (190–1000 nm) that there is no detectable

alteration of the PTFE optical properties produced by electron irradiation. This is evident by the superposition of the spectra collected from the irradiated PTFE samples with the spectrum collected from the pristine PTFE film. This also suggests that the C=C units formed (as detected *via* infrared spectroscopy) are isolated, perhaps in the form of terminal $-CF=CF_2$ groups and not as main chain conjugated double bonds identified in the irradiated polyethylene samples.

Polystyrene

Physical structure. The commercial PS film acquired for the present experiments is atactic (*i.e.* the random orientation of consecutive monomer units) with a completely amorphous distribution of chains. For this reason, complications in assigning vibrational frequencies due to neighboring chain interactions, often associated with crystalline polymers, is not observed in the IR spectra obtained from PS samples.²⁵ It can then be assumed that the experimental FTIR spectrum consists of peaks derived from vibrations of the PS monomer alone. However, the presence of the phenyl group (C_6H_5 , approximating the structure of a monosubstituted benzene ring) in the repeating monomer unit, which possesses a total of 30 normal vibrational modes, results in a spectrum rich in absorption bands. As the ring deformation and bending modes of the monosubstituted benzene ring vibrate at frequencies lower than 2000 cm^{-1} , it is often the case that absorption bands in the spectrum overlap in the congested mid-IR region. In addition, modes of the same symmetry species in a monosubstituted benzene ring can display mixing, which results in a ‘borrowing’ of absorption intensity between the vibrations. After considering the C–H stretching fundamentals of the monosubstituted benzene ring between 3000 and 3150 cm^{-1} , the end result is a PS spectrum that closely resembles that of pure benzene (C_6H_6). The main difference between the PS and the benzene spectra being the fundamentals associated with the internal modes of the hydrocarbon chain, all of which are IR active but absorb at varying intensities.

Infrared spectroscopy. The FTIR spectra of 300 K PS films irradiated with 5 keV (1.0 μA) electrons over 3 hours is displayed in Fig. 2 (bottom). Irradiation experiments using the same electron energy were also conducted at 10, 100, and 200 K. However, irradiation at these lower temperatures did not induce any new absorption features in the IR spectra, so discussion will be limited to the 300 K experiments shown in Fig. 2. Immediately apparent is a decrease ($\sim 1/3$) in intensity for the strongest absorption bands when comparing the IR spectrum collected before irradiation with the spectra collected during electron irradiation. As the PS sample is amorphous, a loss of structural order is unlikely to be the cause of this intensity reduction. However, this observation may indicate a substantial decrease in absorbing species, brought about by the loss of atomic constituents in the PS material *via* electron irradiation. The positions of the absorption bands correlate well with the fundamental frequencies located in the literature³² and compiled in Table 7. Various absorption bands pertaining to the phenyl ring deformation modes $\nu(\text{Ph})$ are observed in close proximity below 2000 cm^{-1} , while

Table 7 Vibrational assignments of polystyrene (PS)

Absorption/cm ⁻¹	Irradiation absorption/cm ⁻¹	Literature value ^a /cm ⁻¹	Assignment ^a	Characterization
542	511	—	—	—
620	—	540	$\nu_4(\text{B}_2)$	Out-of-plane deformation
705	650	622	$\nu_{6\text{B}}(\text{B}_1)$	In-plane bend
761	723	—	—	—
843	—	700	$\nu_{11}(\text{B}_2)$	Out-of-plane deformation
907	—	762	$\nu_{10\text{B}}(\text{B}_2)$	Out-of-plane deformation
941	—	842	$\nu_{10\text{A}}(\text{A}_2)$	Out-of-plane deformation
964	—	906	$\nu_{17\text{B}}(\text{B}_2)$	Out-of-plane deformation
1003	—	945	$\nu_4 + \nu_{16\text{A}}$	Combination
1028	—	965	$\nu_{17\text{A}}(\text{A}_2)/\gamma_r(\text{CH}_2)$	–CH ₂ rock
1071	—	—	—	—
1112	—	1027	$\nu_{18\text{A}}(\text{A}_1)$	In-plane CCH bend
1153	—	1070	$\nu'_{18\text{B}}(\text{B}_1)/\nu(\text{CC})$	In-plane CCH bend
1183	—	—	—	—
1311	—	1154	$\nu'_{15}(\text{B}_1)$	In-plane CCH bend
1329	—	1180	$\nu_5 + \nu_{16\text{B}}$	Combination
1371	—	1310	$\nu'_3(\text{B}_1)$	—
1453	—	1328	$\nu_{14}(\text{B}_1)$	—
1492	1464	1376	$\delta(\text{CH}_2)$	–CH ₂ bend
1542	—	1450	$\delta(\text{CH}_2)/\nu_{19}(\text{B}_1)$	–CH ₂ bend/in-plane bend
1582	—	—	—	—
1601	—	1493	$\nu_{19\text{A}}(\text{A}_1)$	In-plane bend
1672	—	1585	$\nu_{9\text{A}}(\text{A}_1)$	In-plane bend
1743	—	1602	$\nu_{9\text{B}}(\text{B}_1)$	In-plane bend
1803	—	1675	$\nu_{10\text{B}} + \nu_{17\text{B}}$	Combination
1871	—	1745	$\nu_{10\text{A}} + \nu_{17\text{B}}$	Combination
1942	—	1800	$\nu_{10\text{A}} + \nu_{17\text{A}}$	Combination
2336	—	1875	$\nu_{17\text{B}} + \nu_5$	Combination
2849	—	1945	$\nu_{17\text{B}} + \nu_5$	Combination
2925	—	—	—	—
3001	—	2851	$\nu_s(\text{CH}_2)$	CH symmetric stretch
3027	—	2923	$\nu_a(\text{CH}_2)$	CH asymmetric stretch
3059	—	3002	—	—
3080	—	3029	$\nu'_{20\text{A}}(\text{A}_1)$	Ph: CH stretch
3102	—	3061	$\nu'_2(\text{A}_1)$	Ph: CH stretch
	—	3083	$\nu_{20\text{B}}(\text{B}_1)$	Ph: CH stretch

^a Liang and Krimm (1958).³²

the C–H stretching modes $\nu(\text{Ph})$ of the phenyl ring are observed to be clustered together between 3029 and 3080 cm⁻¹. For the hydrocarbon backbone, the bending mode $\delta(\text{CH}_2)$ is identified as a strong feature at 1371 cm⁻¹ (and as a possible mixing component of the strong 1453 cm⁻¹ band) while the rocking mode $\gamma_r(\text{CH}_2)$ can be attributed to the weak shoulder located at 964 cm⁻¹. Finally, the intense absorption bands assigned to the symmetric $\nu_s(\text{CH}_2)$ and asymmetric $\nu_a(\text{CH}_2)$ stretching modes of the –CH₂– backbone are identified at 2849 and 2925 cm⁻¹ respectively.

During the electron irradiation of the PS samples at 300 K, a number of new absorption features arose in the 2000–400 cm⁻¹ IR region. They are identified in Fig. 2 (bottom, right) where spectra are shown over 1 hour intervals. The irradiation induced peaks located at 511, 650 and 723 cm⁻¹ are all of moderate intensity and are clearly identified amongst their neighboring PS phenyl group deformation bands. In addition, a weak shoulder feature is produced at 1464 cm⁻¹, positioned on the side of the strong $\delta(\text{CH}_2)$ absorption peak. The 511, 650 and 723 cm⁻¹ peaks are of too lower frequency to derive from stretching, bending or rocking modes, which could originate from unsaturation of the PS backbone or any small

hydrocarbons formed *via* irradiation processes. They are more likely to be associated with the ring deformation modes of benzene (C₆H₆) liberated from the PS chain by energetic electron irradiation. Research of literature for aromatic vibrations correlating with these specific infrared frequencies could not produce definitive assignments. However, this may not be surprising, as earlier studies of the low-frequency deformation bands of the aromatic ring structures show particular sensitivity to the molecule's environment and temperature (*i.e.* varying band positions for crystalline C₆H₆ at 77 K,³³ C₆H₆ deposited in Ar and Kr matrices at 25 K³⁴ and C₆H₆ dimers in PS films³⁵). Vibrational modes of aromatic molecules are strongly influenced by neighboring aromatic species in disordered systems, such as the amorphous PS microstructure at 300 K investigated in the present study. Therefore, it is probable that any dissociated C₆H₆ produced from the irradiation of PS, which is unable to diffuse from the disordered polymer environment, would experience considerable perturbation to their normal vibration modes. This effect would result in a shift of the absorption band position away from its expected position in the mid-IR spectrum. It is therefore proposed that the 511, 650 and 723 cm⁻¹ absorption

bands identified in the spectrum for the PS film irradiated at 300 K originate from the perturbed ring deformation vibrations of trapped C_6H_6 groups.

Mass spectrometry. Fig. 3 (bottom) displays the recorded mass spectrum for a 300 K PS film irradiated with 5 keV electrons (1.0 μ A) for 3 hours. The mass spectra recorded for this experiment displayed an increase in ion current at mass/charge ratios attributed to H_2^+ ($m/z = 2$), benzene ($C_6H_6^+$; $m/z = 78$) and the benzene fragment $C_6H_5^+$ ($m/z = 77$; not shown). There is no observation of these products for the lower temperature irradiation experiments conducted at 10, 100, and 200 K. The ion current for each species is observed to increase to its maximum value immediately after irradiation exposure. The peak ion current is measured to be 1.8×10^{-12} A and 3.7×10^{-12} A for H_2^+ and $C_6H_6^+$ respectively. Over the 3 hour irradiation period, these ion currents are observed to decrease in an exponential-like decay. The benzene ion current decreases at a faster rate than the molecular hydrogen signal, which may indicate that benzene produced in the subsurface of the PS film has difficulty diffusing through the polymer. In contrast, the spatially smaller hydrogen molecules generated beneath the surface layer are able to diffuse through the PS microstructure more readily and outgas into the UHV chamber for detection by the QMS.

UV-vis spectroscopy. Fig. 4 (bottom) displays the transmission UV-vis spectra for PS films previously irradiated with 5 keV electrons (1.0 μ A) for 3 hours at sample temperatures of 10, 100, 200 and 300 K. Also depicted is the UV-vis spectrum of a PS sample without exposure to electron irradiation. PS films absorb strongly in the far UV region (~ 200 – 400 nm), which is verified in our experimental spectra by the total absorption (corresponding to ~ 4 absorption units) of the incident radiation in this frequency range. This strong absorption characteristic is due to the π - π^* transitions of the PS aromatic ring group; specifically the transitions of the dipolar excited states (< 220 nm) and forbidden transitions of the homopolar excited states (240–270 nm),³⁶ which correspond to the two intense bands observed in Fig. 4. However, it is in the UV region between 250 and 500 nm, depicted in Fig. 4 (bottom, right), where some evidence for irradiation induced modification of the PS film is displayed in the UV-vis spectra. There is a noticeable increase in absorbance for electron irradiated PS samples, correlating with an increase in the temperature of the polymer during irradiation. UV absorption bands between 275 nm and 375 nm can be attributed to π - π^* transitions in $-C=C-$ bonding systems.³⁷ Therefore, the increase in UV absorbance in this region is likely due to an increase in density of conjugated carbon bonds in the PS chain structure, formed after hydrogen atoms are dissociated from the PS by energetic electron interaction. In addition, the density of $-C=C-$ bond centers PS is probably enhanced at irradiation higher temperatures by facilitating diffusion processes for the free hydrogen atoms. An increase in the mobility of hydrogen atoms away from the unsaturated bond centers would reduce the likelihood of back-reactions.

Discussion

Polymer degradation

Polyethylene. The quantitative analysis of HDPE film degradation, induced by exposure to 5 keV electron irradiation at sample temperatures between 10 and 300 K, was performed in two steps. Firstly, the creation of *trans*-vinylene ($-CH=CH-$) species was monitored *in situ* by the growth of the $-CH=CH-$ out-of-plane CH deformation band at 969 cm^{-1} in the experimental FTIR spectra (Fig. 2). Over the 3 hour irradiation period, the 969 cm^{-1} absorption band was integrated and converted to a *trans*-vinylene column density ($[-CH=CH-]$ in molecules cm^{-2}) using the method described in ref. 38. These calculations were performed with a modified Lambert–Beer expression and the integral absorption coefficient ($2.81 \times 10^{-18}\text{ cm molecule}^{-1}$ from the *trans*-vinylene linear absorption coefficient in ref. 39). Fig. 5 displays the temporal profiles of the *trans*-vinylene column densities at 10, 100, 200 and 300 K. For the 300 K experiment, the temporal profile of the $[-CH=CH-]$ column density appears to follow first-order kinetics, supporting an $A \rightarrow B$ reaction pathway (eqn (7)).



$$[-CH=CH-]_t = [-CH_2-CH_2-]_0 \times (1 - e^{-k_1 t}) \quad (8)$$

For the first-order kinetic model (eqn (8)),⁴⁰ we define $[-CH_2-CH_2-]_0$ as the initial column density (molecules cm^{-2}) of HDPE monomer that, over time t (s), is converted to a column density of the *trans*-vinylene species $[-CH=CH-]_t$ at a rate k_1 (s^{-1}). From the (pseudo) first-order curve fitted to the data in Fig. 5 at 300 K, the rate constant was found to be $k_1 = 1.70 \pm 0.01 \times 10^{-3}\text{ s}^{-1}$ (Table 8). In addition, the maximum column density of *trans*-vinylene as $t \rightarrow \infty$ was found to be $6.58 \pm 0.08 \times 10^{15}\text{ molecules cm}^{-2}$.

However, in Fig. 5, the *trans*-vinylene temporal profiles for the lower temperature experiments ($T = 10, 100$ and 200 K) show that the *trans*-vinylene column density decreases after reaching a maximum at $t \approx 2000\text{ s}$. This suggests that the

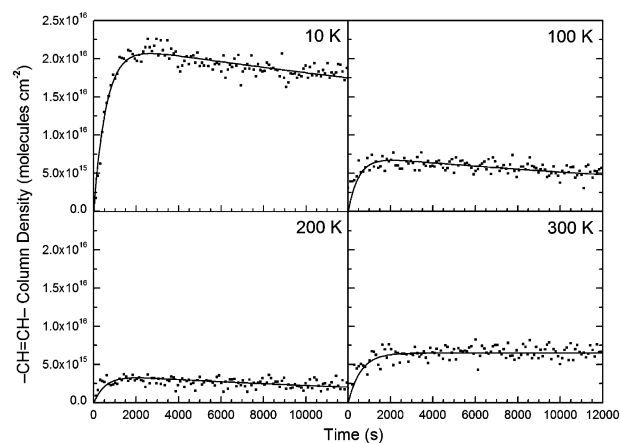
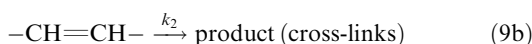
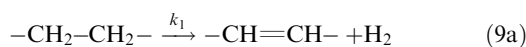


Fig. 5 Fit of the *trans*-vinylene ($-CH=CH-$) column densities for irradiated PE films over a 3 hour exposure period at 10, 100, 200 and 300 K.

Table 8 Kinetic data for Fig. 5

Temperature/K	$[-\text{CH}_2-\text{CH}_2-]_0$ ($\times 10^{15}$ molecules cm^{-2})	k_1 ($\times 10^{-3}$ s^{-1})	k_2 ($\times 10^{-5}$ s^{-1})
10	21.8 ± 0.3	1.70 ± 0.01	1.9 ± 0.2
100	7.20 ± 0.08	2.00 ± 0.01	3.5 ± 2.9
200	3.60 ± 0.05	1.80 ± 0.01	5.0 ± 3.2
300	6.58 ± 0.08	1.70 ± 0.01	—

trans-vinylene species acts as a classical reaction intermediate, being formed and then consumed in a sequential two-step ($A \rightarrow B \rightarrow C$) reaction pathway (eqn (9a) and (9b)). Therefore, a sequential model (eqn (10))⁴⁰ was adopted to fit the profile of *trans*-vinylene abundance ($[-\text{CH}=\text{CH}-]_t$ molecules cm^{-2}) over time, t (s). As a single *trans*-vinylene unit is produced from a single, irradiated HDPE monomer unit (of column density $[-\text{CH}_2-\text{CH}_2-]$ molecules cm^{-2} at $t = 0$), it follows that the rate constant k_1 (s^{-1}) determines the rate of *trans*-vinylene formation (eqn (9a)), while k_2 (s^{-1}) determines the rate of *trans*-vinylene destruction (eqn (9b)).



$$[-\text{CH}=\text{CH}-]_t = [-\text{CH}_2-\text{CH}_2-]_0 \times \frac{k_1}{(k_2 - k_1)} \times (e^{-k_1 t} - e^{-k_2 t}) \quad (10)$$

The fitted curves in Fig. 5 produced an average rate constant of $k_1 = 1.83 \pm 0.01 \times 10^{-3} \text{ s}^{-1}$ (calculated from Table 8) for *trans*-vinylene formation between 10 and 200 K, which was consistent with the $k_1 = 1.70 \pm 0.01 \times 10^{-3} \text{ s}^{-1}$ rate of formation derived at 300 K. However, the rate constants determined for the destruction of the *trans*-vinylene species were observed to be dependent on the temperature of the irradiated HDPE samples and ranged from $k_2 = 1.9 \pm 0.2 \times 10^{-5} \text{ s}^{-1}$ at 10 K to $k_2 = 5.0 \pm 3.2 \times 10^{-5} \text{ s}^{-1}$ at 200 K (Table 8). Showing similar sample temperature dependence, the maximum column density of *trans*-vinylene decreased from $21.8 \pm 0.3 \times 10^{15}$ molecules cm^{-2} at 10 K to $3.60 \pm 0.05 \times 10^{15}$ molecules cm^{-2} at 200 K. The experimental results show no evidence for the formation of a final product species corresponding to the decrease in intensity of the 969 cm^{-1}

absorption peak for the *trans*-vinylene reaction intermediate after $t = 2000$ s. This prevents the development of a full reaction pathway for the lower temperature experiments (eqn (9b)). However, further investigation of the HDPE irradiation results to follow will indicate that carbon-carbon cross-linking is the likely end product at lower sample temperatures.

Summarized in Table 9, the total number of *trans*-vinylene units ($\sum(-\text{CH}=\text{CH}-)$) formed in the irradiated HDPE film, over the exposed surface area ($3.2 \pm 0.5 \text{ cm}^2$), was directly calculated from the maximum column densities of the species $[-\text{CH}=\text{CH}-]_\infty$ (Table 8). The ratio of total *trans*-vinylene units created ($\sum(-\text{CH}=\text{CH}-)$) to the total of original monomer units ($\sum(-\text{CH}_2-\text{CH}_2-)$ units) at each sample temperature was then calculated. It can be observed that the electron irradiation was most “efficient” at lower temperature where, at 10 K, $1.44 \pm 0.49\%$ of the ethylene monomer was converted to a *trans*-vinylene unit by energetic electron interaction. This is opposed to the higher temperature experiments where this percentage was less than 0.5%.

Secondly, the generation of gas phase, molecular hydrogen was quantitatively calculated from the mass spectra displayed in Fig. 3. The total amount of molecular hydrogen was recorded *in situ* during irradiation of the HDPE samples and during the subsequent heating of the films to 300 K. Calibration of the QMS ion current (A) with predetermined pressures of hydrogen gas in the reaction chamber allowed for measurement of the out-gassed molecular hydrogen generated by the irradiation of HDPE. The total abundance of out-gassed molecular hydrogen ($\sum(\text{H}_2)$ in molecules) for each experiment was then derived (Table 9) after correcting for the pumping speed of the species ($S_{\text{eff}}(\text{H}_2) = 770 \text{ L s}^{-1}$) over the total volume (15 L) of the UHV system. The abundance of molecular hydrogen was observed to increase with the irradiated sample temperature from $2.3 \pm 0.3 \times 10^{15}$ molecules at 10 K to $22.0 \pm 2.9 \times 10^{15}$ molecules at 300 K. Subsequently, the ratio of total *trans*-vinylene units formed in the HDPE sample to the total number of hydrogen molecules produced *via* electron irradiation ($\sum(-\text{CH}=\text{CH}-)/\sum(\text{H}_2)$) could then be calculated (Table 9). This ratio was observed to be higher at low temperatures (29.8 ± 8.6 at 10 K) before dropping to a more expected 1 : 1 value of 0.96 ± 0.29 at 300 K. This result is peculiar, as a formation of a *trans*-vinylene double bond in the polymeric chain should produce

Table 9 Calculated abundances and *G*-values for HDPE reactants and products

Temperature/K	$\sum(-\text{CH}_2-\text{CH}_2-)$ ($\times 10^{18}$ units)	$\sum(-\text{CH}=\text{CH}-)$ ($\times 10^{16}$ units)	$\sum(-\text{CH}=\text{CH}-)/\sum(-\text{CH}_2-\text{CH}_2-)$ (%)	<i>G</i> ($-\text{CH}=\text{CH}-$) ($\times 10^{-4}$ units (100 eV) ⁻¹)
10	4.8 ± 0.8	6.98 ± 1.19	1.44 ± 0.49	25.6 ± 8.7
100	4.8 ± 0.8	2.30 ± 0.39	0.48 ± 0.14	8.5 ± 2.9
200	4.8 ± 0.8	1.15 ± 0.19	0.24 ± 0.08	4.2 ± 1.4
300	4.8 ± 0.8	2.11 ± 0.36	0.44 ± 0.15	2.5 ± 0.9

Temperature/K	$\sum(\text{H}_2)$ ($\times 10^{15}$ molecules)	$\sum(-\text{CH}=\text{CH}-)/\sum(\text{H}_2)$	<i>G</i> (H_2) ($\times 10^{-5}$ molecules (100 eV) ⁻¹)
10	2.3 ± 0.3	29.8 ± 8.6	8.6 ± 1.5
100	1.3 ± 0.2	18.3 ± 5.5	4.6 ± 0.8
200	6.3 ± 0.8	1.83 ± 0.54	23.1 ± 3.9
300	22.0 ± 2.9	0.96 ± 0.29	80.8 ± 13.7

a single hydrogen molecule, irrespective of the irradiation temperature.

One plausible explanation for this discrepancy may be the temperature dependence for the cross-linking degradation mechanism of HDPE. Early research⁴¹ into PE irradiation with 800 keV electrons showed that PE samples preferentially undergo cross-linking processes, as opposed to chain-scission. Experimentally, this was quantified by measuring changes in the macroscopic properties of the PE samples post-irradiation, such as swelling and an increased tensile strength. The formation of cross-links between adjacent polymer chains is dependent on the 'mobility' of the chains. At higher sample temperatures HDPE chains 'relax' and become more amorphous and flexible. This increase in mobility promotes the likelihood that two irradiation induced radicals on separate polymer chains can come into contact and form a polymer cross-link. In the context of the present study, the low temperature irradiation of HDPE would result in a small degree of cross-linking, due to the restricted movement of the polymeric chains. This restricted mobility promotes any newly formed radicals to undergo back-reacting processes with free hydrogen atoms. Furthermore, these reverse reactions would continue to propagate until radicals are created on neighboring chain carbons which can then react to form a *trans*-vinylene group on the polymer chain. Inversely, the polymers possess sufficient mobility at higher temperatures to promote chain-linking as the dominant degradation mechanism for the electron irradiated HDPE.

Comparative yields for these degradation processes have been published²¹ for experiments involving the irradiation of PE samples with energetic heavy ions (C^+-Kr^+ ; LET values $>100 \text{ keV } \mu\text{m}^{-1}$) in the form of G -values (number of reactions or events per 100 eV of energy absorbed by the irradiated material). These have been reported for molecular hydrogen formation, $G(H_2) = 3.3 \text{ molecules } (100 \text{ eV})^{-1}$; for chain scission, $G(X) = 2.7 \text{ events } (100 \text{ eV})^{-1}$ and for *trans*-vinylene species formation $G(-CH=CH-) = 0.8 \text{ units } (100 \text{ eV})^{-1}$. G -values for the current set of experiments have also been calculated (Table 9) where:

$$G(H_2): 8.6 \pm 1.5 \times 10^{-5} (10 \text{ K}) - 80.8 \pm 13.7 \times 10^{-5} (300 \text{ K}) \text{ molecules } (100 \text{ eV})^{-1} \quad (11)$$

and

$$G(-CH=CH-): 25.6 \pm 9.8 \times 10^{-4} (10 \text{ K}) - 2.5 \pm 0.9 \times 10^{-4} (300 \text{ K}) \text{ units } (100 \text{ eV})^{-1} \quad (12)$$

As the LET calculated for 5 keV electrons is low ($6.7 \pm 0.2 \text{ keV } \mu\text{m}^{-1}$), the small G -values determined for the present experiments are reasonable when compared with the previously reported G -values; recall that these G values were derived from experiments involving irradiation with energetic heavy ions that often possess high LET values and hence can induce more damage.⁴²

Polytetrafluoroethylene. Previous studies^{22,43} investigating PTFE exposed to various forms of ionizing radiation have supplied evidence that PTFE undergoes main chain scission as a primary degradation process. This chain scission process was

observed to promote the formation of terminal $-CF=CF_2$ groups and the generation of fragment species such as CF_2 , CF_4 and C_2F_6 .²¹ The results from the present study also indicate that chain scission is the prominent degradation process for PTFE irradiated with 5 keV electrons. The mid-IR spectrum (Fig. 2) clearly displays an increase in absorption for both the terminal vinyl ($-CF=CF_2$ at 1791 cm^{-1}) and *trans*-vinylene ($-CF=CF-$ at 1735 cm^{-1}) groups over the three hour irradiation period. The mass spectra (Fig. 3) recorded evidence for dissociated CF_3 radicals out-gassed at 200 K by the identification of its electron ionization fragments CF , CF_2 , CF_3 in expected relative abundances by their peak ion currents (A). In addition, significant amounts of atomic fluorine were detected by the QMS at all irradiated sample temperatures. The UV-vis spectra recorded post-irradiation (Fig. 4) showed no evidence for conjugated systems formed in the PTFE films. However, this can be accounted for if the terminal vinyl groups created by the chain scission process are the more abundant chromophore species, compared to main chain *trans*-vinylene, in the irradiated PTFE microstructure. Terminal vinyl groups require UV frequencies higher than the 190 nm spectrometer limit to detect $\pi-\pi^*$ excitation, hence they cannot be observed to increase in density within our irradiated PTFE samples. This is opposed to conjugated chain *trans*-vinylene groups which absorb lower frequency light and should be observed over the UV range in the experimental spectra.

As an integrated absorption coefficient for the 1791 cm^{-1} $-CF=CF_2$ absorption band could not be located in the literature, quantitative analysis of the terminal vinyl group column densities in the PTFE sample could not be performed. Instead, Fig. 6 displays the temporal growth of the integrated 1791 cm^{-1} vinyl peak area over time, t (s). A first-order growth model (eqn (13))⁴⁰ was then used to fit the increase in area of the IR vinyl absorption ($[-CF=CF_2]$ in cm^{-1}), after conversion from an original amount of PTFE monomer units ($[-CF_2-CF_2]_0$ in cm^{-1}), at rate k_3 (s^{-1}).

$$[-CF=CF_2]_t = [-CF_2-CF_2]_0 \times (1 - e^{-k_3 t}) \quad (13)$$

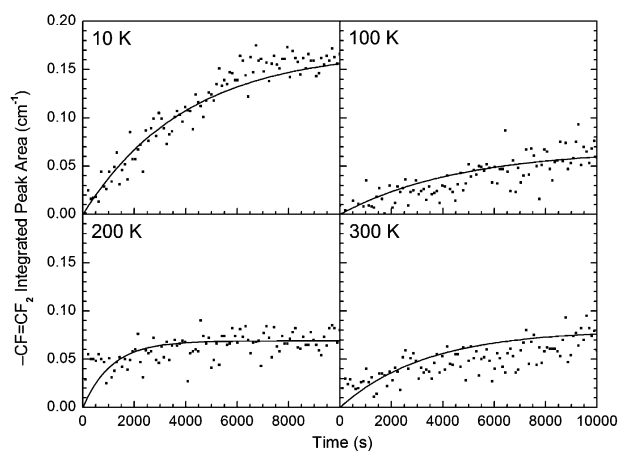


Fig. 6 Fit of the terminal $-CF=CF_2$ (1790 cm^{-1}) integrated peak areas in electron irradiated PTFE films over a 3 hour exposure period at 10, 100, 200 and 300 K.

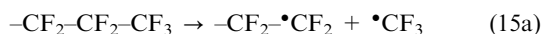
Table 10 Kinetic data for Fig. 6

Temperature/K	$[-CF_2-CF_2]_0$ ($\times 10^{-2}$ cm $^{-1}$)	k_3 ($\times 10^{-4}$ s $^{-1}$)
10	17.0 ± 2.9	2.5 ± 0.9
100	6.7 ± 1.6	2.1 ± 1.2
200	6.8 ± 0.2	9.0 ± 1.4
300	8.0 ± 0.2	3.0 ± 0.9

The kinetic curves constructed in Fig. 6 display an average rate of $k_3 = 4.15 \pm 1.41 \times 10^{-4}$ s $^{-1}$ (calculated from Table 10) for vinyl group formation over the 10–300 K temperature range. This first-order exponential growth model, when applied to the temporal vinyl absorption band profile, supports the reaction pathway depicted in eqn (14). Here, although energetic electron exposure cleaves the PTFE chain at a random carbon–carbon bond, resulting in the formation of two terminal $-CF=CF_2$ groups and two fluoride radicals for the single irradiation event, each $-CF_2-CF_2-$ monomer unit results in a single terminal vinyl group after the loss of a fluoride radical. This preference for PTFE to undergo chain scission is expected as the high electron affinity of fluorine allows the polymeric fluorine atoms to scavenge the secondary electrons generated in the irradiation. From here, the carbon–fluorine bond of PTFE can be cleaved, leading to the release of the fluorine radical or fluoride ion.



In addition, a similar reaction pathway (eqn (15a) and (15b)) associated with the polymeric chain end-groups is proposed to account for the dissociation of $^{\bullet}CF_3$ fragments, which were identified in the QMS spectra recorded for the PTFE sample irradiated at 200 K (Fig. 3). Here, a vinyl end group is established following the release of a CF_3 radical and an F atom in a sequential process.



Polystyrene. Even though PS displays high resistance to irradiation induced degradation due to the protective nature of its phenyl groups, some evidence for chemical change initiated by 5 keV electron exposure has been observed in the current set of experiments. New mid-IR absorption bands in the 1600–400 cm $^{-1}$ region (Fig. 2), thought to originate from dissociated aromatic species trapped in the PS microstructure, have been observed to arise in absorption intensity at 300 K. In addition, the corresponding mass spectrum (Fig. 3) detected gaseous hydrogen and benzene molecules evolved from the 300 K sample; note that a peak at $m/z = 78$ alone can be any C_6H_6 isomer; only the identification of benzene in the infrared spectrum assigns signal at $m/z = 78$ to benzene. The UV-vis spectra collected from the irradiated PS films (Fig. 4) also showed a temperature dependent increase in chromophore density in the 300–400 nm region. Previous studies^{44,45} investigating the effects of electron irradiation on PS have determined that PS undergoes cross-linking as primary degradation process. However, the radiation resistance of the polymer is further reflected in the small molecular

hydrogen yields published for the polymer ($G(H_2) = 0.026$ molecules (100 eV) $^{-1}$ at 393 K in air²⁰).

The lack of new absorption features in the PS mid-IR spectra prevented any quantitative modeling on the formation of unsaturated chain groups as performed with the HDPE and PTFE samples. In addition, the QMS ion current could not be correlated to partial pressure of gas phase benzene in the experimental chamber, precluding the calculation of the total number of benzene molecules sputtered from the PS surface at 300 K. However, after adopting the same method used for calculating the abundance of molecular hydrogen generated from the irradiated HDPE samples detailed above, a total number of $2.16 \pm 0.37 \times 10^{16}$ molecules of hydrogen were calculated to be evolved from PS at 300 K, over the 3 hour irradiation period. This abundance corresponds to a $G(H_2) = 7.95 \pm 2.70 \times 10^{-5}$ molecules (100 eV) $^{-1}$.

Conclusions

Before we discuss potential implications of our research, it is important to summarize the results of our experiments (Table 11; Fig. 7).

Polyethylene

(1) FTIR: The FTIR depicts the formation of *trans*-vinylene groups at temperature independent rates ($k = 1.80 \pm 0.01 \times 10^{-3}$ s $^{-1}$). During the irradiation, *trans*-vinylene intensity displays a temperature dependent decrease between 10 and 200 K, indicating cross-linking may be an alternative degradation pathway at higher doses.

(2) QMS: A temperature dependent evolution of molecular hydrogen ($G(H_2) = \sim 10^{-4}$ – 10^{-3} molecules (100 eV) $^{-1}$) could be monitored.

(3) UV-vis: An increase in absorption above 400 nm due to π – π^* transitions in newly formed conjugated systems is evident.

Polystyrene

(1) FTIR: We identification benzene trapped in polymer network at 300 K.

(2) QMS: The evolution of molecular hydrogen ($G(H_2) = 7.95 \pm 2.70 \times 10^{-5}$ molecules (100 eV) $^{-1}$) and benzene (at 300 K) was evident.

(3) UV-vis: An increase in 275–375 nm absorption region due to π – π^* transitions suggests the formation of extended conjugated π systems.

Table 11 Summary of irradiation induced polymer alteration observed in Results section

	FTIR	QMS	UV-vis
Polyethylene	<i>trans</i> -Vinylene (–CH=CH–)	H ₂	π – π^*
Polytetrafluoroethylene	<i>trans</i> -Vinylene (–CF=CF–) Terminal vinyl (–CF=CF ₂)	F CF ₃ (200 K)	—
Polystyrene	Benzene (300 K)	H ₂ (300 K) C ₆ H ₆ (300 K)	π – π^*

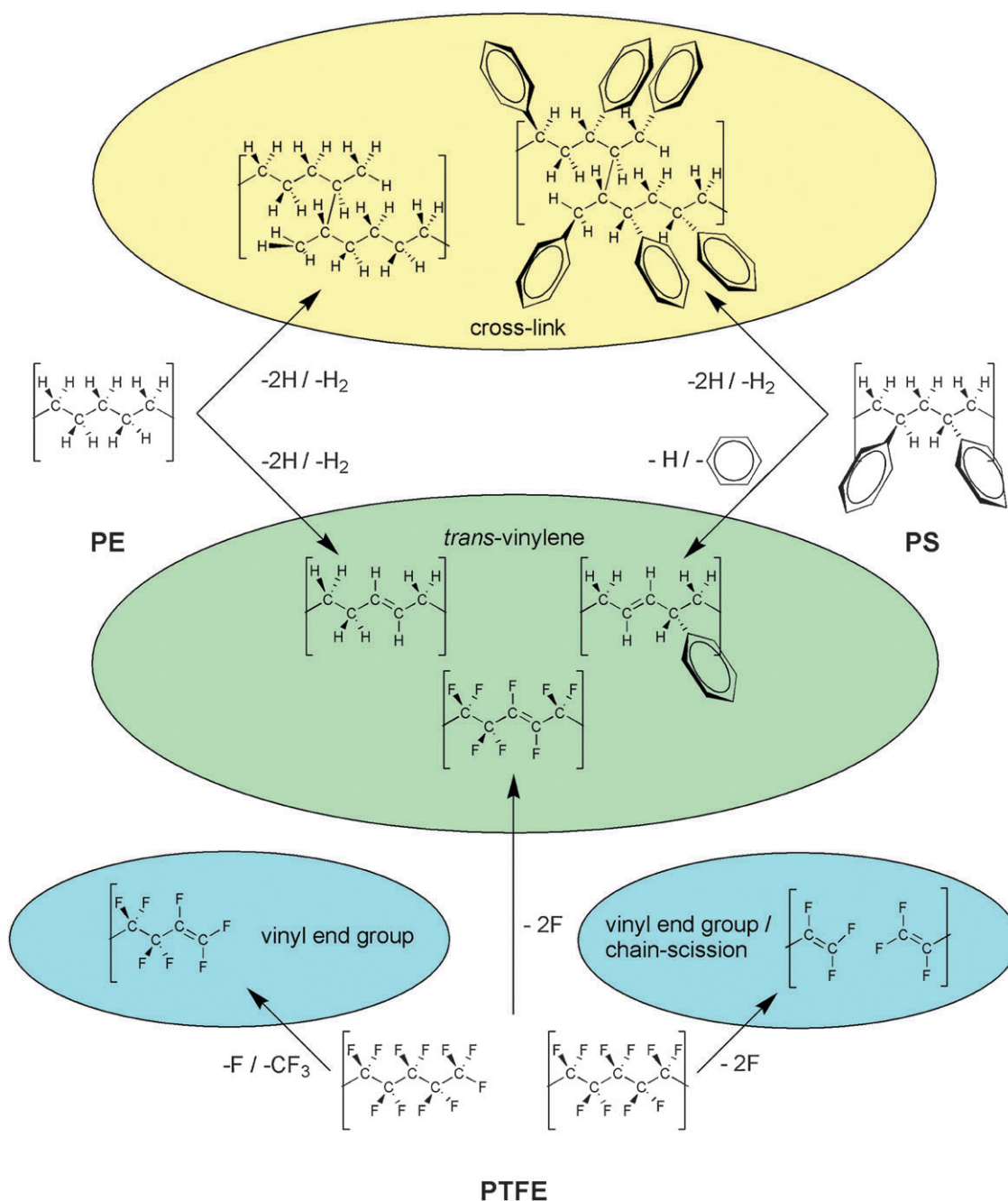


Fig. 7 Overview of polymer degradation mechanisms induced by energetic electrons.

Polytetrafluoroethylene

(1) FTIR: The formation of *trans*-vinylene and vinyl end-groups is evident. The intensity of vinyl end-group 1790 cm^{-1} mid-IR absorption peak increases with a temperature independent rate ($k = 4.15 \pm 1.41 \times 10^{-4}\text{ s}^{-1}$). Observation of vinyl end-group absorption band indicates PTFE undergoes chain-scission.

(2) QMS: Temperature and electron current dependent evolution of atomic fluorine at all experimental temperatures and the detection of CF_3 radicals at 200 K are verified.

(3) UV-vis: The absence of absorption increase in π - π^* region verifies preferential formation of vinyl end-group over conjugated main-chain groups.

These results as summarized above suggest that aliphatic, substituted polymers such as PE and PS as well fluorinated polymers (PTFE) have a common decomposition mechanism *via* the formation of *trans*-vinylene bonds ($-CX=CX-$). In addition, PS and PE degrade *via* cross-linking releasing molecular hydrogen (PE/PS) and benzene (PS). Finally, PTFE shows distinct reaction pathways generating terminal vinyl groups ($-CF=CF_2$) as well as fluorine atoms and CF_3 groups; the absence of molecular fluorine might be attributed to the fact that fluorine hardly diffuses in the polymer, but on the other hand, hydrogen atoms generated in PS and PE can easily recombine even at 10 K.

These results have important implications. The radiation induced degradation of polymeric materials is a concern for

aerospace design when operating in the harsh LEO and near-Earth space environments. In the context of extended manned missions like the ISS, material integrity is paramount for spacecraft longevity and the successful operation of various sub-systems moderating thermal control and the protection of crew from harmful dosages of energetic irradiation. This study has simulated the effect of 5 keV electron irradiation energies that mimic fast secondary electrons, which are formed in the track of highly energetic GCRs penetrating a material (such as GCRs bombarding a spacecraft surface). In comparison to atomic oxygen particles in LEO, which are completely stopped by a 3.5 nm protective layer of Al₂O₃ deposited on a polymer surface,⁴⁶ 5 keV electrons are calculated²³ to lose only ~60 eV of kinetic energy after passing through the same protective coating. This suggests that the remaining 4.94 keV of electron energy is able to generate significant damage to the underlying polymer even if thin coatings are employed to protect a spacecraft from irradiation. This effect is even more dramatic when calculating that GCR particles like MeV or GeV protons or helium nuclei lose less than 1% of their kinetic energy in the Al₂O₃ coating. Therefore, for spacecraft design, it is crucial to discriminate if the spacecraft is operating on LEO, where clearly oxygen atoms are the principal destructive particles, or if the spacecraft is operating in deep space such as extended missions to the Moon or Mars. In these cases, protective layers of Al₂O₃ are not very useful.

The tendency for PTFE to undergo degradation in the near-Earth space environment due to high LET irradiation has been well documented in the case of the Hubble Space Telescope, where PTFE containing materials (*i.e.* aluminized Teflon fluorinated ethylene-propylene), lining the exterior of the spacecraft for thermal insulation purposes, displayed cracking and erosion over the operational lifetime of the spacecraft.⁴⁷ The break-down of the material is expected due to the inherent nature of PTFE to undergo chain scission as a prominent degradation pathway during exposure to ionizing radiation. The results in the present study confirm this, with an IR absorption band assigned to terminal vinyl groups detected in the mid-IR spectrum over the experimental range of irradiation temperatures. These findings display the proliferation of chain scission, even after exposure to low LET electrons in the keV energy range. With every chain scission event, the average molecular weight of macromolecular chain is decreased and the mechanical strength of the PTFE material is reduced accordingly. In addition, the *in situ* detection of substantial amounts dissociated fluorine, evolved as a consequence of the chain scission process and a species known to be highly reactive in its atomic form, could be an additional concern in regards to chemical attack of exterior spacecraft surfaces.

Finally, the present experiments confirm that PS displays a particularly high resistance to irradiation exposure. At 300 K a small degree of out-gassing of molecular hydrogen and benzene was detected by QMS after irradiation of PS with 5 keV electrons. The degree of gas evolution was measured to be ~10 times less than HDPE under the same irradiation conditions at 300 K. PS preferentially forms cross-links as a primary degradation pathway which resulted in no noticeable formation of unsaturated centers in the polymeric chain by

FTIR spectroscopy and only a slight increase in chromophore concentration by UV-vis spectroscopy. For these reasons PS appears to be a more suitable material than HDPE for radiation shielding. This is due to the presence of the energy dissipating aromatic rings in the PS monomer unit limiting irradiation induced damage to the polymer microstructure and subsequently reducing the amount of molecular hydrogen gas generated by energetic electrons.

Acknowledgements

This project was supported by Air Force Office of Scientific Research (A9550-09-1-0177). We thank Dr Chris Bennett, UH, for valuable discussions.

References

- 1 P. B. Willis and C. H. Hsieh, *Kobunshi*, 2000, **49**, 52.
- 2 M. L. Everett and G. B. Hoflund, *Macromolecules*, 2004, **37**, 6013.
- 3 J. W. Wilson, F. A. Cucinotta, J. L. Shinn, L. C. Simonsen, R. R. Dubey, W. R. Jordan, T. D. Jones, C. K. Chang and M. Y. Kim, *Radiat. Meas.*, 1999, **30**, 361.
- 4 M. R. Shavers, N. Zapp, R. E. Barber, J. W. Wilson, G. Qualls, L. Toupes, S. Ramsey, V. Vinci, G. Smith and F. A. Cucinotta, *Adv. Space Res.*, 2004, **34**, 1333.
- 5 C. D. Li, D. Z. Yang, S. Y. He and S. Q. Yang, *J. Spacecr. Rockets*, 2004, **41**, 373.
- 6 G. W. Nam, C. W. Kong, Y. M. Yi and A. Ohnishi, *Thermochim. Acta*, 2009, **494**, 123.
- 7 A. R. Chambers, I. L. Harris and G. T. Roberts, *Mater. Lett.*, 1996, **26**, 121.
- 8 G. D. Badhwar, *Radiat. Res.*, 1997, **148**, S3.
- 9 D. N. Baker, *Adv. Space Res.*, 1998, **22**, 7.
- 10 E. Grossman and I. Gouzman, *Nucl. Instrum. Methods Phys. Res., Sect. B*, 2003, **208**, 48.
- 11 X. H. Zhao, Z. G. Shen, Y. S. Xing and S. L. Ma, *Polym. Degrad. Stab.*, 2005, **88**, 275.
- 12 K. B. Shin, C. G. Kim, C. S. Hong and H. H. Lee, *Composites, Part B*, 2000, **31**, 223.
- 13 E. R. Benton and E. V. Benton, *Nucl. Instrum. Methods Phys. Res., Sect. B*, 2001, **184**, 255.
- 14 C. J. Bennett, S. H. Chen, B. J. Sun, A. H. H. Chang and R. I. Kaiser, *Astrophys. J.*, 2007, **660**, 1588.
- 15 J. Cazaux, *J. Phys. D: Appl. Phys.*, 2005, **38**, 2433.
- 16 T. E. Madey, R. E. Johnson and T. M. Orlando, *Surf. Sci.*, 2002, **500**, 838.
- 17 G. Rostoker, S. Skone and D. N. Baker, *Geophys. Res. Lett.*, 1998, **25**, 3701.
- 18 D. N. Baker, S. G. Kanekal, X. Li, S. P. Monk, J. Goldstein and J. L. Burch, *Nature*, 2004, **432**, 878.
- 19 M. J. Roedel, *J. Am. Chem. Soc.*, 1953, **75**, 6110.
- 20 D. W. Clegg and A. A. Collyer, *Irradiation Effects on Polymers*, Elsevier Science Publishers LTD, New York, 1991.
- 21 D. Fink, *Fundamentals of Ion-Irradiated Polymers*, Springer Publishing, New York, 2004.
- 22 U. Lappan, U. Geissler and K. Lunkwitz, *J. Appl. Polym. Sci.*, 1999, **74**, 1571.
- 23 D. Drouin, A. R. Couture, R. Gauvin, P. Hovington, P. Horny and H. Demers, *Monte Carlo Simulation of Electron Trajectory in Solids (CASINO) ver 2.4.2.*, Univ. Sherbrooke, Quebec, 2002.
- 24 S. Krimm, C. Y. Liang and G. B. B. Sutherland, *J. Chem. Phys.*, 1956, **25**, 549.
- 25 D. I. Bower and W. F. Maddams, *The Vibrational Spectroscopy of Polymers*, Cambridge University Press, New York, 1989.
- 26 A. A. Abdel-Fattah, S. Ebraheem, Z. I. Ali and F. Abdel-Rehim, *J. Appl. Polym. Sci.*, 1998, **67**, 1837.
- 27 D. M. Bodily and M. Dole, *J. Chem. Phys.*, 1966, **45**, 1428.
- 28 J. Davenas and P. Thevenard, *Nucl. Instrum. Methods Phys. Res., Sect. B*, 2003, **208**, 170.
- 29 R. E. Moynihan, *J. Am. Chem. Soc.*, 1959, **81**, 1045.
- 30 C. Y. Liang and S. Krimm, *J. Chem. Phys.*, 1956, **25**, 563.

- 31 G. Masetti, F. Cabassi, G. Morelli and G. Zerbi, *Macromolecules*, 1973, **6**, 700.
- 32 C. Y. Liang and S. Krimm, *J. Polym. Sci.*, 1958, **27**, 241.
- 33 J. L. Hollenberg and D. A. Dows, *J. Chem. Phys.*, 1962, **37**, 1300.
- 34 K. G. Brown and W. B. Person, *Spectrochim. Acta, Part A*, 1978, **34**, 117.
- 35 S. Chattopadhyay and A. Datta, *Chem. Phys. Lett.*, 2004, **391**, 216.
- 36 L. Calcagno, G. Compagnini and G. Foti, *Phys. Rev. B: Condens. Matter*, 1992, **46**, 10573.
- 37 L. Singh and K. Singh Samra, *Radiat. Phys. Chem.*, 2008, **77**, 252.
- 38 C. J. Bennett, C. Jamieson, A. M. Mebel and R. I. Kaiser, *Phys. Chem. Chem. Phys.*, 2004, **6**, 735.
- 39 J. F. Rabek, *Polymer Photodegradation: Mechanisms and Experimental Methods*, Chapman & Hall, New York, 1994.
- 40 J. I. Steinfeld, J. S. Francisco and W. L. Hase, *Chemical Kinetics and Dynamics*, Prentice-Hall, Upper Saddle River, 1989.
- 41 E. J. Lawton, P. D. Zemaný and J. S. Balwit, *J. Am. Chem. Soc.*, 1954, **76**, 3437.
- 42 M. Mélot, Y. Ngono-Ravache and E. Balanzat, *Nucl. Instrum. Methods Phys. Res., Sect. B*, 2003, **209**, 205.
- 43 U. Lappan, U. Geissler and U. Scheler, *Macromol. Mater. Eng.*, 2007, **292**, 641.
- 44 V. Švorčík, V. Rybka, V. Hnatowicz, M. Novotna and M. Vognar, *J. Appl. Polym. Sci.*, 1997, **64**, 2529.
- 45 M. Ferry, Y. Ngono-Ravache, V. Picq and E. Balanzat, *J. Phys. Chem. B*, 2008, **112**, 10879.
- 46 R. Cooper, H. P. Upadhyaya, T. K. Minton, M. R. Berman, X. Du and S. M. George, *Thin Solid Films*, 2008, **516**, 4036.
- 47 K. K. De Groh, J. A. Dever, J. K. Sutter, J. R. Gaier, J. D. Gummow, D. A. Scheiman and C. He, *High Perform. Polym.*, 2001, **13**, 401.
- 48 T. F. Williams and M. Dole, *J. Am. Chem. Soc.*, 1959, **81**, 2919.
- 49 H. Y. Kang, O. Saito and M. Dole, *J. Am. Chem. Soc.*, 1967, **89**, 1980.
- 50 D. C. Waterman and M. Dole, *J. Phys. Chem.*, 1970, **74**, 1913.
- 51 D. C. Waterman and M. Dole, *J. Phys. Chem.*, 1971, **75**, 3988.
- 52 K. Prošková, V. Švorčík, V. Rybka and V. Hnatowicz, *Radiat. Phys. Chem.*, 2000, **58**, 153.
- 53 H. M. A. Zeid, Z. I. Ali, T. M. A. Maksoud and R. M. Khafagy, *J. Appl. Polym. Sci.*, 2000, **75**, 179.
- 54 A. Kondyurin, R. Khaybullin, N. Gavrilov and V. Popok, *Vacuum*, 2002, **68**, 341.
- 55 S. Makkonen-Craig, M. Paronen, K. Arstila, K. Helariutta, E. Rauhala and P. Tikkanen, *Nucl. Instrum. Methods Phys. Res., Sect. B*, 2005, **236**, 366.
- 56 Z. I. Ali, *J. Appl. Polym. Sci.*, 2007, **103**, 3461.
- 57 R. Singh, K. S. Samra, R. Kumar and L. Singh, *Radiat. Phys. Chem.*, 2008, **77**, 53.
- 58 M. E. Martínez-Pardo, J. Cardoso, H. Vazquez and M. Aguilar, *Nucl. Instrum. Methods Phys. Res., Sect. B*, 1998, **140**, 325.
- 59 S. Massey, P. Cloutier, M. Bazin, L. Sanche and D. Roy, *J. Appl. Polym. Sci.*, 2008, **108**, 3163.
- 60 L. Singh, K. S. Samra, R. Singh, I. Solania and D. K. Avasthi, *J. Non-Cryst. Solids*, 2008, **354**, 41.
- 61 D. Fischer, U. Lappan, I. Hopfe, K. J. Eichhorn and K. Lunkwitz, *Polymer*, 1998, **39**, 573.
- 62 J. Tian and Q. Xue, *J. Appl. Polym. Sci.*, 1998, **69**, 435.
- 63 G. Peng, D. Yang and S. He, *Polym. Adv. Technol.*, 2003, **14**, 711.
- 64 R. Kumar, S. A. Ali, A. K. Mahur, H. S. Virk, F. Singh, S. A. Khan, D. K. Avasthi and R. Prasad, *Nucl. Instrum. Methods Phys. Res., Sect. B*, 2008, **266**, 1788.